Title
Frustrated Magnets: Topology, Bose-Einstein Condensation, and Order-by-disorder

Author
Flynn, Michael Owen

Publication Date
2021

Peer reviewed|Thesis/dissertation

Frustrated Magnets: Topology, Bose-Einstein Condensation, and Order-by-disorder

By

MICHAEL FLYNN
DISSERTATION

Submitted in partial satisfaction of the requirements for the degree of

DOCTOR OF PHILOSOPHY

in

Physics

in the

OFFICE OF GRADUATE STUDIES

of the

UNIVERSITY OF CALIFORNIA

DAVIS

Approved:

Rajiv R.P. Singh (Chair)

Mukund Rangamani

Daniel L. Cox

Committee in Charge

2021

Abstract

If a single phrase can be said to embody modern perspectives on many-body theory, it is P.W. Anderson's famously simple line, "More is different". This idea is well understood by practitioners of many-body theory, and field theory more generally, as drawing a distinction between the degrees of freedom which define a macroscopic system and the emergent degrees of freedom which control its low-energy behavior. This dissertation will center this concept by studying a set of models – frustrated magnetic systems – which maximize the distinction between effective and definitional degrees of freedom. Each model highlights distinct sets of "exotic" many-body phenomena.

We begin by considering an insulating quantum magnet on the geometrically frustrated kagomè lattice. A simple approximation to the physics of some materials, such as the iron jarosites, is achieved by focusing on nearest-neighbor antiferromagnetic exchange and spin-orbit effects in the form of Dzyaloshinskii-Moriya interactions. Through series expansions around the strong-field limit, we will provide evidence that this model generically realizes either topological magnon bands or "semimetals" built out of charge-neutral magnetic excitations. We will also use the wavefunctions computed in this process to determine transport functions of interest, such as the thermal Hall conductivity. In the topological phase, we compute the system's Chern numbers and discuss the consequences of topological phase transitions for transport properties.

Next, we consider intriguing empirical results for the Lanthanide-based compound Ytterbium Silicate ($Yb_2Si_2O_7$). This quantum dimer magnet is related to other well-known materials which exhibit Bose-Einstein condensation transitions of spin excitations when subjected to a magnetic field. We construct an effective spin model which reproduces the observed behavior of $Yb_2Si_2O_7$, and use a broad range of computational techniques to argue that this model captures

the essential physics of the material. This example highlights the prospect of producing novel interacting phases in materials with strong spin-orbit coupling.

Finally, we consider the statistical mechanics of a model that we call the distorted pyrochlore Heisenberg model. This model constitutes a thermodynamic interpolation between the kagomé and pyrochlore Heisenberg models, which each have storied histories in the context of spin liquid physics. We will argue that thermal order-by-disorder – a phenomenon present in the kagomé, but absent in the pyrochlore – appears above a nonzero transition temperature in a quasi-two dimensional limit. We discuss the thermodynamic signatures of this behavior in the low-temperature limit and their relevance for layered kagomé systems.

Acknowledgments

I would like to begin by acknowledging my Ph.D. adviser, Rajiv Singh, for his persistent guidance over the last six years. With his assistance, I have learned a great deal about the theory of frustrated magnets and condensed matter theory more generally. Further, he has generously introduced me to the broader condensed matter community by providing opportunities to attend conferences and participate in collaborations. Our work is supported in part by National Science Foundation Division of Materials Research Grant number 1855111.

A number of other faculty at the University of California, Davis have been very generous with their time, providing me with helpful discussions and other forms of support in recent years. This includes Mukund Rangamani, Veronika Hubeny, Andrew Essin, and Eduardo da Silva-Neto. At Stanford University, I have also benefitted from a number of conversations with Xiao-Liang Qi and his collaborators, particularly Daniel Ranard. I would also like to thank my collaborator, Thomas Baker, for his assistance on a broad range of problems over the last three years.

For the work of Chapter 3, I would also like to acknowledge my collaborator, Siddharth Jindal, and the experimentalists Kate A. Ross and Jeffrey Quilliam. Truly, the work in that chapter could not have been completed without the impressive experimental work of their groups.

Finally, I would like to thank my mother, Joan, and partner, Lauren, for their persistent support while completing this process. Prioritizing education for such an extended period of time can feel like a selfish endeavor, but they never stopped encouraging me to keep going.

Table of Contents

List of Figures

Chapter 1

Magnetism, Quantum and Classical

1.1 Introduction: Why Magnets?

All undergraduate physics students become acquainted with the basic theory of magnetism fairly early in their studies. Beyond the physics of magnetic dipoles, one might wonder how much there is to learn about this subject. After all, it's often said that magnetic forces were known to the ancient Greeks; how much novelty could possibly be left in such a storied field? Setting aside the significant exercises in mathematical physics one performs in electromagnetism courses, what else is there to see? Furthermore, are there any general lessons to learn at all? One might worry that most of the research into magnetism today is narrowly focused on individual materials which are deemed empirically interesting. While the study of individual materials is a worthwhile pursuit, theoretical physicists would generally prefer to develop paradigm-defining principles which put those examples in a broader framework. This is certainly the prevailing attitude found in other areas of physics, popularized by the modern perspective associated with the renormalization group and effective field theory [2–4].

The reader can be forgiven for asking such questions: condensed matter physics is a massive field, and identifying the physical themes underlying such a large volume of work is a nontrivial task. While it can seem at times that there is a "zoo" of results which defy attempts to develop a unified perspective, history has demonstrated that condensed matter systems can be understood through a principled theoretical approach. Examples of these unifying theories in many-body physics include the theory of Fermi liquids, the Landau-Ginzburg theory of symmetry

breaking phase transitions, and the theory of topological order [5–9]. We will hopefully convince the reader over the course of this dissertation that condensed matter physics, and the theory of magnetic systems in particular, is an extraordinarily rich field with many general lessons in store for its practitioners.

One of the goals of this dissertation is to highlight some of the active themes of many-body research in the context of specific problems. For example, Chapter 3 is motivated by interesting empirical data for a particular compound, Ytterbium Silicate ($Yb_2Si_2O_7$). The spin model that we will construct in order to understand that data is closely related to other spin models which exhibit Bose-Einstein condensation of magnetic excitations. This class of models, which are applicable to a broad range of materials, illustrate a prevailing theme of modern condensed matter theory: mappings between very different models can yield deep insights, and in some cases exact solutions.

The rest of this chapter is used to provide short introductions to some of the central concepts we will encounter throughout the dissertation. While this commentary is brief, it should provide adequate motivation for our technical decisions going forward. The interested reader is urged to consult the enclosed references for more details.

1.2 Band Topology

Topology has come to play an extremely important conceptual role in modern condensed matter physics. While the advent of topology in many-body physics is somewhat novel from a historical perspective, today it is used to characterize a broad range of many-body phenomena. This includes the use of topological invariants as clear diagnostics of phases of matter, such as topological insulators, and the theory of fractionalized quasiparticles in two dimensional systems [10, 11]. In fact, topology's role is so prevalent in condensed matter theory today that the term is overloaded - there are multiple, conceptually distinct, applications of topology which appear in different physical contexts.

Here we will briefly review the manifestation of topology which we will encounter in Chap-

ter 2, namely, the role of topology in band theory. Historically, this subject gained significant attention for its role in studies of the integer quantum Hall effect. The most striking property of integer quantum Hall systems is the sharp quantization of the Hall conductivity in units of e^2/h. That a many-body response function could be so precisely quantized, despite empirical effects such as disorder, is remarkable. Such a remarkable feature is in need of a remarkable explanation.

This explanation came from Thouless, Kohmoto, Nightingale, and den Nijs (TKNN) [12]. We will briefly summarize their argument. Suppose we have a translation-invariant many-body system, so that wavefunctions are labeled by momentum $\mathbf{k}$ and take the Bloch form

$$\psi_{\mathbf{k}}(\mathbf{x}) = e^{i\mathbf{k}\cdot\mathbf{x}} u_{\mathbf{k}}(\mathbf{x}) \tag{1.1}$$

where $u_{\mathbf{k}}(\mathbf{x})$ has the periodicity of a unit cell. This generically divides the spectrum into well-defined energy bands separated by gaps. Note that the Brillouin zone in which we define our momenta is topologically non-trivial in two dimensions - it is a torus. Adiabatic transport of an arbitrary initial state around the Brillouin zone yields a wavefunction that differs from the initial state by a phase. Aside from an uninteresting dynamical phase associated with adiabatic transport, there may be a geometric component to the phase factor (also known as the Berry phase). In discussions of the Berry phase, it is natural to define a Berry connection over the Brillouin zone:

$$A_j(\mathbf{k}) = -i\langle u_{\mathbf{k}} | \partial_{k_j} | u_{\mathbf{k}} \rangle \tag{1.2}$$

This connection provides a measure of how much a wavefunction $u_{\mathbf{k}}(\mathbf{x})$ "twists" as it is wound around the Brillouin zone. However, the connection is "gauge dependant" in the sense that it is sensitive to phase conventions for the Bloch states. Clearly, any quantity which depends on our choice of phase for the basis states cannot be physically relevant. A gauge-invariant quantity one can build from the Berry connection is the Berry curvature,

$$F(\mathbf{k}) = \frac{\partial A_x}{\partial k_y} - \frac{\partial A_y}{\partial k_x} \tag{1.3}$$

This is clearly reminiscent of the situation in electromagnetism, where we are taught to build the field-strength tensor from the vector potential. A topological invariant known as the first Chern number or TKNN invariant comes from the integral of the curvature:

$$C = -\frac{1}{2\pi} \int_{\text{B.Z.}} d\mathbf{k}\ F(\mathbf{k}) \in \mathbb{Z} \tag{1.4}$$

where the integral is over the Brillouin zone. This integer-valued invariant is part of a larger story in mathematical physics that we will not explore further [13, 14]. Remarkably, this classification of maps over the Brillouin zone is physically significant: the TKNN invariant is directly related to the Hall conductivity of the integer quantum Hall effect, as one can show from textbook linear response arguments. For our purposes in Chapter 2, we will be studying excitations about a field-polarized magnet rather than free fermions. In this context, the Chern number is still a useful topological invariant, and we will study it in relation to a new response function, the thermal Hall conductivity.

1.3 Comments on Computational Methods

In subsequent chapters, we will use a number of computational techniques which have become standard practice in many-body theory. For the sake of pedagogical completeness, the following sections are used to introduce the core ideas underlying these methods.

1.3.1 Mean-Field Theory and Spin-Wave Theory

Mean-field theory is a general approach to many-body problems that seeks to replace an interacting Hamiltonian with a set of effective single-particle problems. This is typically achieved by using an ansatz for an ordered state to decouple the Hamiltonian, which renders the problem soluble with standard methods. The parameters of the decoupling ansatz are then constrained to match the single-particle solution, and a self-consistent result is achieved [6, 15].

It is, of course, profoundly naive to expect that neglecting interactions will have no qualitative (let alone quantitative) impact on the results of our analysis. As a prototypical example, let us consider a classical nearest-neighbor model with antiferromagnetic coupling on an arbitrary lattice:[1]

$$H = \sum_{\langle ij \rangle} J \mathbf{S}_i \cdot \mathbf{S}_j \tag{1.5}$$

We might anticipate that at low temperatures, the ground state of (1.5) spontaneously breaks some symmetries and exhibits long-range magnetic order. If the system "freezes" into such a configuration, an expansion in fluctuations is often reasonable. This can be implemented by rewriting

$$\mathbf{S}_i = \langle \mathbf{S}_i \rangle + (\mathbf{S}_i - \langle \mathbf{S}_i \rangle) \equiv \langle \mathbf{S}_i \rangle + \delta \mathbf{S}_i \tag{1.6}$$

The expectation value $\langle \mathbf{S}_i \rangle$ represents our ansatz for the ordered phase, and can be quite complicated in systems with a large unit cell. We will encounter an example with a simple but non-trivial unit cell in Section 3.2.3. Substituting (1.6) into (1.5) and neglecting quadratic terms in fluctuations, we find

$$H = \sum_{\langle ij \rangle} J \left[\langle \mathbf{S}_i \rangle \cdot \mathbf{S}_j + \mathbf{S}_i \cdot \langle \mathbf{S}_j \rangle - \langle \mathbf{S}_i \rangle \cdot \langle \mathbf{S}_j \rangle \right] \tag{1.7}$$

Now we can compute the single-spin expectation values from (1.7) and insist that they match the form postulated in our ansatz. When neglect of fluctuations is qualitatively justified, this mean-field scheme does a reasonable job of estimating the location of phase boundaries and the nature of the phase transitions associated with them. However, such calculations should not be trusted without further support from unbiased methods.

One can systematically build upon mean-field theory by studying fluctuations around the

[1] This is a very glib description, as the lattice structure often controls the accuracy of mean-field theory. Neglect of fluctuations is more controlled for systems with a large coordination number (particularly in higher dimensions) or on a bipartite lattice. Here we are being very schematic.

mean-field solution. There are a number of techniques which are well-suited to this purpose; later, we will encounter one in the study of spin-waves, the Holstein-Primakoff transformation [16]. This method maps the fluctuations of spins onto bosons, using the large value S of an ordered spin moment to control a $1/S$ expansion. Explicitly, the transformation is given by

$$\begin{aligned} S^z &= S - a^\dagger a \\ S^+ &= \sqrt{2S - a^\dagger a}\ a \\ S^- &= a^\dagger \sqrt{2S - a^\dagger a} \end{aligned} \tag{1.8}$$

This is supplemented by the non-holonomic constraint $0 \leq a^\dagger a \leq 2S$. Replacing spins with bosons might seem bizarre at first glance, but such a representation is natural due to the fact that Pauli matrices for spins on different sites commmute. Several variations on this idea exist, including bosonic representations with holonomic constraints (Schwinger bosons) and even fermionic representations [7, 17–19].

The Holstein-Primakoff transformation can be used to study the role of spin-wave corrections to an ordered state. Using the replacement (1.8), we can expand S^+ and S^- in powers of $a^\dagger a/S$. At the quadratic level, the boson problem can be diagonalized using Bogoliubov transformations, and the resulting band structure yields insights into, for example, scattering properties [20, 21]. We will use this expansion in Section 3.2.2 to reproduce neutron scattering data in the compound Ytterbium Silicate.

1.3.2 Matrix Product State Methods

From a computational perspective, the fundamental difficulty of many-body quantum mechanics is the fact that Hilbert space grows exponentially as a function of system size. More concretely, since our interest will be concentrated on insulating systems built out of electrons, we consider a system of N spin-1/2 degrees of freedom on the sites of an arbitrary lattice. The Hilbert space $\mathcal{H}$ of this system has a dimension given by

$$\dim(\mathcal{H}) = 2^N \tag{1.9}$$

Given a Hamiltonian H, condensed matter physicists are typically interested in finding its ground state and low-lying excitations. From this perspective, the exponential growth of Hilbert space is extraordinarily concerning: for a generic interacting problem, what hope is there of recovering a unique vector in such a massive space? Furthermore, we have argued up to this point that thermodynamically large systems are governed by emergent, collective degrees of freedom that cannot necessarily be observed in small systems. It seems at first glance that computational efforts are doomed, in the sense that only systems of a sufficient size are qualitatively useful.

While this is a daunting prospect – and remains so despite the massive amount of research in quantum many-body theory – physical principles can be used to significantly reduce these computational difficulties. There are, of course, symmetries in many systems which can significantly constrain the results of computations [22]. Another fundamental principle which radically simplifies quantum mechanics is locality. Often the term locality is used to refer to the fact that typical interactions are only strong at short-range. However, our use of the term in this context refers to the fact that interactions typically couple a small number of local Hilbert spaces in each term. For example, even the long-ranged Coulomb interaction is only defined between *pairs* of charged particles. Restricting the Hamiltonian to be a sum of terms that only act on a small number of local Hilbert spaces significantly restricts the sector of the many-body Hilbert space that needs to be considered. In fact, for broad classes of problems, significant evidence has been established which shows that the overwhelming majority of quantum states cannot be eigenstates of local Hamiltonians [23–25].

In light of these facts, it is clear that significant progress can be made with a computational method that takes advantage of locality and the tensor-product structure of Hilbert space. Such a formalism is furnished by the theory of tensor networks, which are a class of ansatzes for many-body wavefunctions [26]. Among these, the best developed are the so-called Matrix Product States (MPS) which are known to faithfully represent the low-energy eigenstates of a signifi-

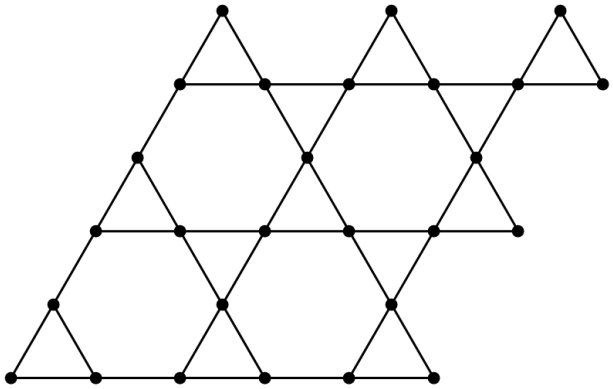

Figure 1.1: A section of the geometrically frustrated kagomé lattice. The kagomé is a two dimensional lattice of corner-sharing triangles.

cant class of physical Hamiltonians [27]. Moreover, there is a highly developed computational algorithm – the Density Matrix Renormalization Group (DMRG) – which provides a variational scheme for optimizing MPS [28]. We will encounter DMRG in Section 3.2.4, where we will use it to quantitatively support a set of results derived from mean-field theory.

1.4 Frustration and the breakdown of mean-field theory

We have already commented on the basic structure of mean-field theory in Section 1.3.1. While mean-field theory is a useful tool, we are of course particularly interested in situations where it breaks down. In the context of magnetism, an interesting approach to breaking down mean-field theory is to study geometrically frustrated systems. These are lattice systems whose geometric structure is incommensurate with the local energetic constraints of a model Hamiltonian [29].

For antiferromagnetic spin models, frustration arises on lattices with triangular motifs. For example, we could consider an antiferromagnetic Ising model on the kagomé lattice (shown in figure 1.1). Around a triangular plaquette, it is necessarily the case that at least two spins on that plaquette will be parallel. Our inability to find a configuration which satisfies all local energetic constraints is a consequence of geometric frustration. More generally, competing long- and short-range interactions will also lead to frustration.

In this context, it is clear that the best one can hope to do is to frustrate one bond per kagomé

triangle. However, for a general finite size system, it is not at all obvious how close one can get to this lower bound on the energy. Moreover, the fact that these constraints are violated locally suggests that the degeneracy of low-energy states could be very large. Indeed, there are a number of frustrated systems for which the ground state degeneracy grows exponentially with system size [30].

It is unsurprising that mean-field theory breaks down in this context. In particular, the utility of the replacement (1.6) depends on the fact that $\langle \mathbf{S} \rangle$ is nonzero. In a system with a massive ground state degeneracy, it is not at all obvious that order of any kind will be established. For the most dramatic cases, such as quantum spin liquids, all local order parameters vanish identically, and mean-field theory must be abandoned [7]. In those cases, it is clear that an inherently many-body description is necessary – a single-particle treatment is simply inappropriate.

In quantum systems, such a large ground state degeneracy provides an ideal environment to observe quasiparticle fractionalization. A well studied example of this phenomenon occurs in the quantum spin-ice model, whose emergent low-energy theory is a deconfined U(1) lattice gauge theory [31]. It is not a coincidence that geometrically frustrated magnets, defined by their inability to satisfy all local energetic constraints, give rise to gauge theories [32, 33]. A closely related phenomena occurs in the theory of topological order, illustrated by Kitaev's toric code [34]. In that case, the number of ground states is controlled solely by topological considerations and is independent of system size. However, each ground state is a massive superposition of macroscopically distinguishable states. It is on top of this highly-entangled, fluctuating background that the anyons of the toric code are stabilized and deconfined [11].

From these examples, we can see that highly degenerate ground state spaces often lead to interesting physics. Chapter 4 studies a classical model with this structure. Although less exotic than their quantum mechanical counterparts, frustrated classical systems exhibit a remarkable sensitivity to fluctuations. A particular interest of ours will be the phenomenon of "order by disorder", which occurs when a subset of ground states is selected by thermal or quantum mechanical fluctuations. We will discuss this phenomena in kagomé and pyrochlore antiferromagnets, and

analyze a model which interpolates between both.

Chapter 2

High-Field Expansions for Kagome Antiferromagnets with Spin-Orbit Coupling [1]

2.1 Introduction

In recent decades, the search for novel many-body phenomena in frustrated systems has been a major focus of condensed matter physics [35–38]. Exotic phases of matter formed due to the interplay of various physical interactions can be delicate, which requires theorists to consider models with a range of perturbations. One such perturbation is Spin-orbit coupling (SOC), which enters the Hamiltonian of insulating magnets via Dzyaloshinskii-Moriya interactions (DMI) [39, 40].

SOC has recently garnered increased attention [41–44]. Experimental efforts to artificially control SOC are an important aspect of spintronics [45, 46], and the competition between geometric frustration, SOC, and various symmetry-breaking perturbations has proven to contain rich physics [47–50]. In such systems spin-wave theory has been used to extract the spectrum of quasiparticles (particularly magnons), yielding a host of predictions for insulating ferromagnets and antiferromagnets, with and without DMI. Through these calculations, the theory of magnon transport has been refined and various experimental probes of topological order have been proposed.

[1] This chapter is adapted from the published work, *High-field expansion approach to kagome antiferromagnets with Dzyaloshinskii-Moriya interactions* , Michael O. Flynn and Rajiv R.P. Singh, Phys. Rev. B **100**, 121108(R) (2019).

Despite the successes of spin-wave theory, the approach has some limitations. Linearization of effective magnon Hamiltonians can forbid certain processes and leaves out terms that may alter magnon spectra and wavefunctions, particularly for small values of the effective spin. It is also important to move beyond single-magnon bands and study the physics of multi-magnon states. Directly addressing spin-half systems would open the possibility of studying multiparticle inelastic scattering processes and bound states in realistic systems.

This chapter takes a different approach to the physics of strongly correlated magnetic systems, built from many-body perturbation theory. While perturbation theory has obvious limitations, it removes the linearization inherent to spin-wave theory. The work presented here focuses on single-magnon states, which allows us to make contact with previous studies of similar models. Multi-magnon states can also be incorporated naturally into this formalism.

In this chapter, we consider a model of localized spin-$1/2$ particles on the kagomé lattice in high magnetic fields. We consider nearest neighbor antiferromagnetic exchange and DMI with in-plane and out-of-plane components. This model, while simple, contains two non-trivial phases. The first, which is a magnetic analog of a Dirac semimetal, contains Dirac points in the magnon spectrum. Importantly, these Dirac points are robust against arbitrary DMI and can be manipulated in principle with modern spintronics techniques. The second phase has bulk band gaps, but has localized conducting modes on its surface when the model is studied with a boundary. This suggests the presence of topological order, so we compute the bulk topological invariant (the band Chern numbers) and the thermal Hall conductivity, which is expected to be nonzero in a topological phase. The Hamiltonian reads

$$H = -\sum_i \mathbf{B}\cdot\mathbf{S}_i + \sum_{\langle ij\rangle}\left[J\mathbf{S}_i\cdot\mathbf{S}_j + \mathbf{D}_{ij}\cdot(\mathbf{S}_i\times\mathbf{S}_j)\right] \tag{2.1}$$

Here $\mathbf{B}$ is the magnetic field, $\langle ij\rangle$ denotes nearest neighbors, $J > 0$ is the antiferromagnetic Heisenberg coupling, and $\mathbf{D}_{ij}$ is the DM vector on the bond ij [51–63]. We will treat the spin interactions as perturbations to the magnetic field coupling; this is valid in the polarized phase. Remaining in the polarized phase roughly requires that $|\mathbf{B}| \gtrapprox (J + |\mathbf{D}|)/3$, but more

precisely corresponds to magnon bands without a zero-energy mode [64]. Figure 2.1 shows our DMI conventions and reviews the lattice structure.

Studies of similar models have been conducted previously, outside of the high-field regime. Mook et. al. [65] considered a ferromagnetic version of (2.1) with next nearest neighbor (NNN) exchange. Laurell and Fiete [66] carried out a spin-wave analysis of the antiferromagnetic version of the same model. The NNN exchange used in these works provides a mechanism for the experimentally observed (weak) dispersion in the bottom band of a Kagome system, which would otherwise be flat [67–69]. Although we do not explicitly include NNN interactions, our approach ultimately produces dispersion in every band. This is because the effective single-particle problem generated by our analysis gives rise to long-ranged hopping of quasiparticles (see section 2.2). Degeneracies in our band structures should therefore be taken seriously, despite the simplicity of (2.1).

The rest of the chapter is organized as follows. In section 2.2, we will review the graphical linked cluster technique and explain how the bands of the model (2.1) are calculated. Section 2.3 presents our results in the case of a magnetic field in the Kagome plane. The resulting phase is a magnonic Dirac semi-metal with Dirac points that can be manipulated by tuning the magnetic field or DMI. Section 2.4 introduces an out-of-plane magnetic field, which breaks the symmetry protecting the Dirac points and gaps the spectrum. There we calculate the magnon thermal Hall conductivity, the Chern numbers of each band, and map out a topological phase diagram using the bulk invariant.

2.2 Linked Cluster Expansion

We will employ the linked cluster expansion technique to derive the properties of single-magnon states. Here we will sketch the technique and establish notation; we refer the reader elsewhere for more details and proofs of our statements [70–73]. We begin by considering a model of spins on a lattice $\mathcal{L}$ with Hamiltonian

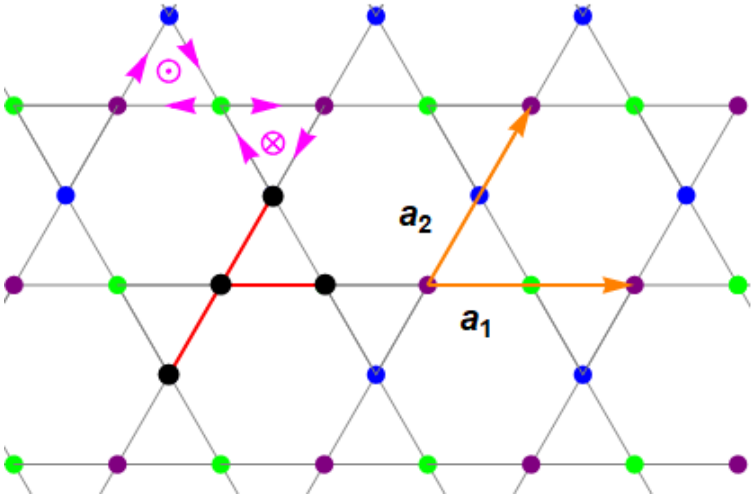

Figure 2.1: A section of the Kagome lattice. Spins are colored according to their sublattice, and an example of a connected graph with three bonds is highlighted (red). This graph has six (proper, connected) subgraphs. We fix the lattice spacing so that the Bravais lattice vectors are given by $\mathbf{a}_1 = (2, 0, 0), \mathbf{a}_2 = (1, \sqrt{3}, 0)$ (orange). Our convention for the Dzyaloshinskii-Moriya vector is shown in purple: cross products are oriented along indicated link directions, the out-of-plane component D_z alternates between plaquettes, and the in-plane component D_p (not shown) points outward from plaquette centers on the bonds of the lattice.

$$H = H_0 + \lambda H_1 \tag{2.2}$$

where H_0 is a solvable Hamiltonian, λ is a small parameter, and H_1 is a non-trivial perturbation. In our case, $1/|\mathbf{B}|$ plays the role of λ, and the unperturbed Hamiltonian is that of non-interacting spins in a magnetic field. The key to our analysis is to identify physical observables whose properties in the thermodynamic limit can be systematically understood by studying finite subsystems of $\mathcal{L}$. Define a connected cluster $c \subset \mathcal{L}$ to be an embedding of a connected graph into $\mathcal{L}$ (see figure 2.1). The cluster c inherits a cluster Hamiltonian H_c by setting the couplings between all spins in c and the remainder of the lattice to zero.

Let $P(\mathcal{L})$ be some physical property for the full lattice model, such as the ground state energy. Such a property can be computed on a cluster c, $P(c)$, using standard perturbation theory. For a generic physical property, computing $P(c)$ reveals little about $P(\mathcal{L})$. However, we will only consider properties which satisfy the following relation:

$$P(A+B) = P(A) \oplus P(B) \tag{2.3}$$

This is the so-called cluster addition property, and it guarantees that we only need to consider connected clusters. One proceeds by defining the weight of a cluster, $W(c)$,

$$W(c) = P(c) - \sum_{g \subset c} W(g) \tag{2.4}$$

where g indexes all (proper, connected) subclusters of c. In our case, the weight of a cluster with n bonds will only contribute at order λ^n due to the subgraph subtraction. Therefore, given a list of all connected graphs which have embeddings in $\mathcal{L}$ along with their multiplicities, we can compute $P(\mathcal{L})$ to arbitrarily high orders.

The discussion thus far works as described for simple extensive properties such as the ground state energy. In general however we are interested in studying the excitations induced by H_1 about the ground state of H_0. For this purpose, the constraint (2.3) seems too strong: there is nothing preventing a quasiparticle from hopping between disconnected clusters. Moreover the number of excitations is not generally conserved unless it happens to be protected by a symmetry of H. Both problems are present in the model (2.1). We can circumvent the latter difficulty by generating effective Hamiltonians on subgraphs of $\mathcal{L}$ which forbid mixing between sectors with different quasiparticle numbers. This is done by finding a unitary transformation U which block diagonalizes the cluster Hamiltonian H_c:

$$H_{\text{eff}} = U^\dagger H_c U \tag{2.5}$$

The transformation U is constructed perturbatively in λ, so that H_{eff} self-consistently forbids mixing up to a given order in perturbation theory. This allows us to study the single-particle band structure in spite of the lack of quasiparticle conservation.

The possibility of excitations hopping between disconnected clusters is still present. To avoid this we need to find a property related to the spectrum which satisfies (2.3). Define $E_1(\mathbf{i}, \mathbf{j}) =$

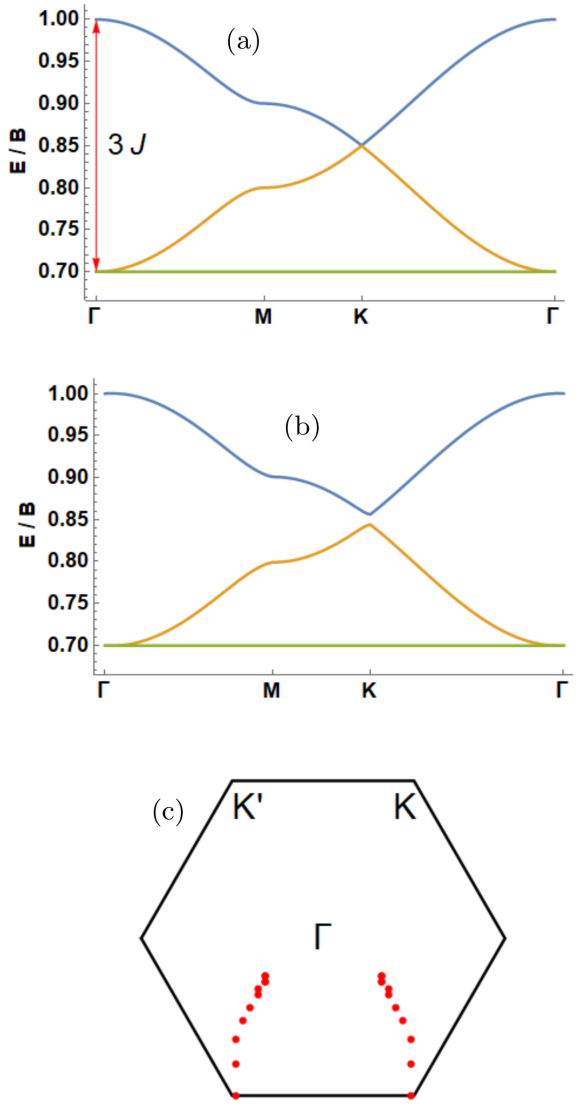

Figure 2.2: The band structure of (2.1) for $\mathbf{B} = B\hat{x}, J = |\mathbf{B}|/10$ and various choices of DMI. (a): Without DMI, the band structure has Dirac points at $\mathbf{K}, \mathbf{K}'$ and a dispersionless band. (b): Introducing out-of-plane DMI ($|\mathbf{D}| = J/10$) does not affect the Dirac points but the previously flat band becomes weakly dispersive (not visible). An in-plane component ($D_p = D_z$) of the DMI shifts the Dirac nodes off of high-symmetry points but does not gap the spectrum. (c): The spread of Dirac points as $\mathbf{D}$ is rotated into the plane. The nodes are displaced symmetrically about the magnetic field axis and orthogonal to it. These points are generated with ten uniformly spaced angular orientations of $\mathbf{D}$ in $[0, \pi/2]$. We set $|\mathbf{D}| = 3J$ for visual effect.

$\langle \mathbf{i}|H_{\text{eff}}|\mathbf{j}\rangle$ to be the hopping matrix element for a single particle state between sites $\mathbf{i}$ and $\mathbf{j}$. Then the following quantity has the cluster addition property:

$$\Delta_1(\mathbf{i},\mathbf{j}) = E_1(\mathbf{i},\mathbf{j}) - E_0\delta_{\mathbf{i},\mathbf{j}} \tag{2.6}$$

where E_0 is the ground state energy of the cluster. We will only deal with systems invariant under translations by Bravais lattice vectors, which leads us to consider momentum eigenstates (N is the number of lattice sites),

$$|\mathbf{k}\rangle = \frac{1}{\sqrt{N}} \sum_{\mathbf{j}} \exp\left(i\mathbf{k}\cdot\mathbf{j}\right)|j\rangle \tag{2.7}$$

In general (and indeed for the kagomé), we must allow for the possibility that the unit cells of $\mathcal{L}$ contain multiple sites. Let δ_{ab} denote the vector connecting two sites of the lattice in sublattices a and b respectively (for the Kagome lattice, $a, b = 1, 2, 3$). Then the band structure of the quasiparticles is obtained by making use of the translation invariance of Δ_1:

$$\omega_1^{ab}(\mathbf{k}) = \sum_{\delta_{ab}} \Delta_1(\delta_{ab})\left[\cos\left(\mathbf{k}\cdot\delta_{ab}\right) + i\sin\left(\mathbf{k}\cdot\delta_{ab}\right)\right] \tag{2.8}$$

Diagonalizing this matrix yields the band structure. This procedure generates effective tight binding Hamiltonians for one-particle excitations. In the case of the model (2.1), we find that all of the matrix elements $E_1(\mathbf{i},\mathbf{j})$ are generically nonzero at sufficiently high orders in perturbation theory. This is a reflection of the strongly correlated nature of the magnons in this problem, and allows a model without explicit NNN exchange to capture details of the band structure of realistic systems.

2.3 Tunable Dirac Points

In this section we take the magnetic field to lie in the kagomé plane, and unless otherwise mentioned we will let $\mathbf{B} = \hat{x}$ (this choice is not essential to the qualitative physics). In the absence of DMI and above the saturation field, the spectrum is known to contain a flat band at finite energy

and two dispersive bands with Dirac points at $\mathbf{K} = \left(\frac{\pi}{3}, \frac{\pi}{\sqrt{3}}\right), \mathbf{K}' = \left(-\frac{\pi}{3}, \frac{\pi}{\sqrt{3}}\right)$ [74–76] (figure 2.2). The tight binding model for the single magnon sector in this case involves only nearest-neighbor hopping.

Upon introducing DMI, the model develops dispersion in each band. We find that the hopping amplitudes satisfy

$$\Delta_1(\delta_{ab}) = \Delta_1^*(-\delta_{ab}) = \Delta_1(\delta_{ba}) \tag{2.9}$$

This result is consistent with a ground state order which is spin-polarized along an axis in the kagomé plane. Combined with (2.8), this implies that $\omega_1^{ab}(\mathbf{k})$ is purely real. This result is manifest when the DMI points out of the kagomé plane, since the Hamiltonian is real; the extension to arbitrary DMI is less obvious. This implies that any effective two-band Hamiltonian obtained by projecting out the third band has an expansion of the form

$$H_{2\times 2}(\mathbf{k}) = E_0 + h_x(\mathbf{k})\,\sigma_x + h_z(\mathbf{k})\,\sigma_z \tag{2.10}$$

where $h_x(\mathbf{k}), h_z(\mathbf{k})$ are real-valued functions and $E_0 > 0$ is a constant energy shift. Perturbations which preserve (2.10) are not expected to gap the Dirac points, which is consistent with our findings: tuning the relative magnitude of the in-plane (D_p) and out-of-plane (D_z) DMI shifts the Dirac points off of high-symmetry lines but never gaps them. The direction of displacement for the Dirac points also depends on the magnetic field orientation. This is to be contrasted with the typical result that SOC gaps out Dirac points, demonstrated for example in graphene.

2.4 Topological Magnon Bands & Chern Numbers

With a magnetic field out of the Kagome plane, all lattice directions in the bulk are equivalent, and

$$\Delta_1(\delta_{ab}) = \Delta_1(-\delta_{ab}) = \Delta_1^*(\delta_{ba}) \tag{2.11}$$

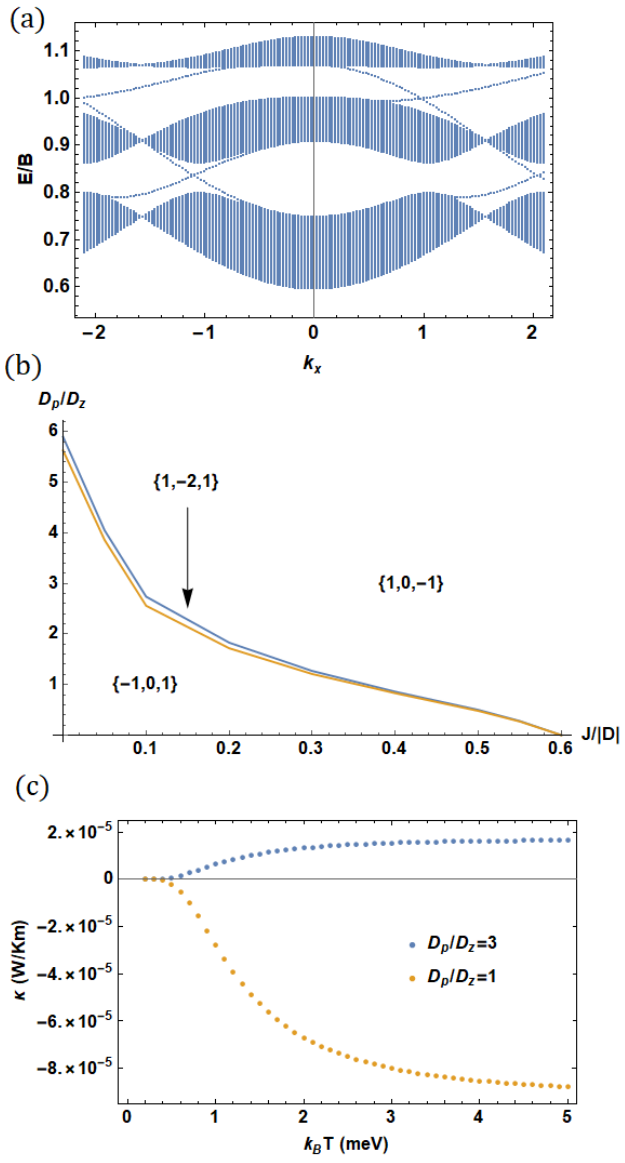

Figure 2.3: (a): Band structure for a semi-infinite system. The modes winding between the bulk bands are exponentially localized on the system's edges. (b): Phase diagram obtained by computing the band Chern numbers. We have chosen $J + |\mathbf{D}| = |\mathbf{B}|/5$. Different parameter choices only adjust the location of the phase boundary. The precise location of the phase boundaries is less significant than the necessary existence of small energy gaps near the transitions. The Chern numbers are indicated in each region from the highest to lowest energy bands; the set $\{1, -2, 1\}$ describes the narrow region in parameter space indicated by the arrow.(c): Thermal Hall conductivity for $J/|\mathbf{D}| = 1/3$ both above and below the transition. We set the magnon energy scale to 5 meV in the absence of interactions, and $J + |\mathbf{D}| = 1$ meV. Hence $|\mathbf{D}| = 0.75$ meV and $J = 0.25$ meV here. The results are observed to be reasonably insensitive to this choice. The Hall conductivity changes sign across the transition by varying the ratio D_p/D_z and the curve closer to the transition (yellow) is significantly enhanced due to the smallness of the gap.

More generally, the hopping amplitudes are invariant under rotations which map the Kagome into itself, provided the sublattice structure is properly accounted for. $\omega_1^{ab}(\mathbf{k})$ is no longer real, which violates (2.10). In two dimensions fine tuning is therefore required to find gapless points and a gapped spectrum is anticipated.

Previous work on similar models has found topological order in phases with bulk band gaps, which leads us to study our model on a finite strip. This strip has open boundary conditions, and in this geometry we find clear evidence of localized edge states which cross the bulk band gaps (figure 2.3 a). Such edge states are necessarily associated with a bulk topological invariant, namely the band Chern numbers [77]. We can map out a topological phase diagram at fixed energy by setting $J + |\mathbf{D}|$ to be a constant fraction of $|\mathbf{B}|$ and looking for changes in the Chern numbers (figure 2.3 b). The most common set of Chern numbers is $\{1, 0, -1\}$ (labeled from the highest to lowest energy band). However there is also a phase with Chern numbers $\{-1, 0, 1\}$ separated from the former phase by a narrow region with Chern numbers $\{1, -2, 1\}$. From an empirical perspective, these transitions are significant because vanishing energy gaps typically enhance transport properties. Indeed, we have computed the thermal Hall conductivity and find it is enhanced significantly near the phase boundary (figure 2.3 c). We also see that the thermal Hall conductivity changes sign across the phase boundary.

We compute the thermal Hall conductivity as follows. Letting $\Omega_n^z(\mathbf{k})$ denote the Berry curvature of band n, the (magnon) thermal Hall conductivity at temperature T is given by [78]

$$\kappa_{xy} = -\frac{k_B^2 T}{(2\pi)^2 \hbar} \sum_n \int_{\mathrm{BZ}} \left[c_2 \left[g\left(\epsilon_{nk}\right) \right] - \frac{\pi^2}{3} \right] \Omega_n^z\left(\mathbf{k}\right) d^2k \tag{2.12}$$

where $g(\epsilon_{nk})$ is the usual Bose-Einstein distribution factor. The function $c_2(x)$ is

$$c_2(x) = (1+x)\left[\ln\left(\frac{1+x}{x}\right)\right]^2 - [\ln(x)]^2 - 2\mathrm{Li}_2(-x) \tag{2.13}$$

where $\mathrm{Li}_2(x)$ is the dilogarithm. When stacks of Kagome layers are used with an interlayer spacing ℓ, κ/ℓ is naturally given in W/Km. All values reported here assume $\ell = 5$ angstroms,

which is fairly typical.

The values obtained for the thermal Hall conductivity are comparable to those found in other studies, although we have chosen small values of J and $|\mathbf{D}|$ so that only modest magnetic fields are necessary to polarize the ground state. Specifically, figure 2.3 assumes a magnon energy of 5 meV in the absence of interactions, with $J + |\mathbf{D}| = 1$ meV. The effect of stronger interactions on the thermal Hall conductivity can also be considered, but this necessarily demands a larger saturation field. As a general point, we see that there can be a significant benefit to finding materials which naturally sit near the phase boundaries discussed in figure 2.3. The empirical interest in such a result should be clear to the spintronics community and others working with tunable DMI and other interactions.

2.5 Conclusion and Future Directions

In this chapter, we have considered a "minimal model" of antiferromagnetic spins with SOC. In the absence of DMI, the physics of magnons in the polarized phase is already well understood. This picture becomes significantly richer with the inclusion of DMI because of the coupling it induces between spin-space and real-space. By changing the ground state ordering (in our case, with a magnetic field), this coupling allows us to see qualitatively new physics, particularly more robust and controllable Dirac points.

We have also explored the phase diagram of a polarized magnet, and the presence of topological phase transitions opens up the possibility of finding enhanced response functions. A search for materials which can exhibit these enhanced responses could prove interesting.

As previously mentioned, our technique has the advantage of avoiding any linearization. This means that multi-magnon states can be considered in detail with our technique, enabling the study of bound states and the multi-magnon continuum.

Chapter 3

Bose-Einstein Condensation in $Yb_2Si_2O_7$ [1]

3.1 Empirical motivation

Through pioneering empirical and theoretical studies, models of localized spins have been shown to contain a wealth of familiar and exotic phases of matter. Interesting orders can be achieved by considering models with competing interactions, which naively require the satisfaction of incompatible constraints to achieve a ground state. Nature's creative mechanisms for resolving these tensions within quantum mechanics is responsible for much of the diversity of phenomena observed within many-body theory [2, 11, 35, 79–82].

A clear example of such physics is found in dimer magnets, where antiferromagnetic exchange is brought into tension with polarizing magnetic fields [1, 83–87]. In these systems, spins form a collective paramagnet with zero total spin in the low-field ground state. A simple example of this phenomenon is realized in the antiferromagnetic Heisenberg model on the breathing honeycomb lattice. As illustrated in Fig. 3.1(a), each spin has a preferred neighbor due to lattice distortion. These pairs of spins form the effective (dimer) degrees of freedom which are best used to study the collective paramagnet and neighboring phases.

Applying a magnetic field to the singlet state generically leads to a BEC transition, where a band of triplet excitations becomes degenerate with the $S = 0$ ground state and creates a magnet-

[1] This chapter is adapted from the published work, *Two Phases Inside the Bose Condensation Dome of $Yb_2Si_2O_7$* , Michael O. Flynn, Thomas E. Baker, Siddharth Jindal, and Rajiv R.P. Singh, Phys. Rev. Lett. **126**, 067201 (2021).

ically ordered state. Typically, this ordered state can be understood through spin-wave theory as an XY antiferromagnet which cants with increasing field. In typical experiments [83], it has been found that strengthening this field eventually polarizes the system; no other phase transitions are observed. Recently, experiments on the compound $Yb_2Si_2O_7$ have challenged this paradigm by suggesting the presence of an intermediate magnetic phase with an unknown underlying order [1]. This chapter studies a proposed modification to the Heisenberg model on the breathing honeycomb lattice whose ground state order is consistent with all available thermodynamic and scattering data, and allows for the possibility of such a phase diagram.

On the breathing honeycomb lattice, the Heisenberg model in a magnetic field only realizes the previously mentioned collective paramagnet, canted XY antiferromagnet, and polarized phases. It has been speculated that the physical origin of the interactions responsible for the unexpected magnetic phase is the strong spin-orbit coupling typical of Lanthanide elements, such as Ytterbium. In the presence of strong spin-orbit coupling, projection to the effective spin-1/2 subspace (or lowest Kramers doublet) typically generates anisotropic spin interactions. We will not attempt to construct a microscopic model for $Yb_2Si_2O_7$, focusing instead on a minimal class of anisotropic interactions consistent with the available data. In particular, we will generalize the Heisenberg model by introducing two forms of anisotropy:

$$H = \sum_{\langle ij\rangle,\alpha} J_{ij}^{\alpha} S_i^{\alpha} S_j^{\alpha} - h \sum_{i\in A,\alpha} g_{z\alpha}^{A} S_i^{\alpha} - h \sum_{j\in B,\alpha} g_{z\alpha}^{B} S_j^{\alpha} \tag{3.1}$$

Here i, j index lattice sites, A, B are the honeycomb sublattices, and $\alpha = x, y, z$. The x, y, z directions correspond, respectively, to the $a^*, b = b^*$, and c axes of the C2/m lattice structure. In other words, we are considering an XYZ model for a breathing lattice, and allowing for the possibility that the z-axis is not a principal axis of the g-tensor. The sublattice-dependence of the g-tensor allows for a staggered component $g_{zx}^{A} = -g_{zx}^{B}$, which is essential to the universal physics we will describe. The "minimal model" for the physics of interest is significantly simpler: it is sufficient to take $J_{ij}^{y} > J_{ij}^{x} = J_{ij}^{z}$ (for all i, j) and $g_{zy} = 0$, as y is a principal axis. More precise constraints discussed below are imposed by consistency with experiments.

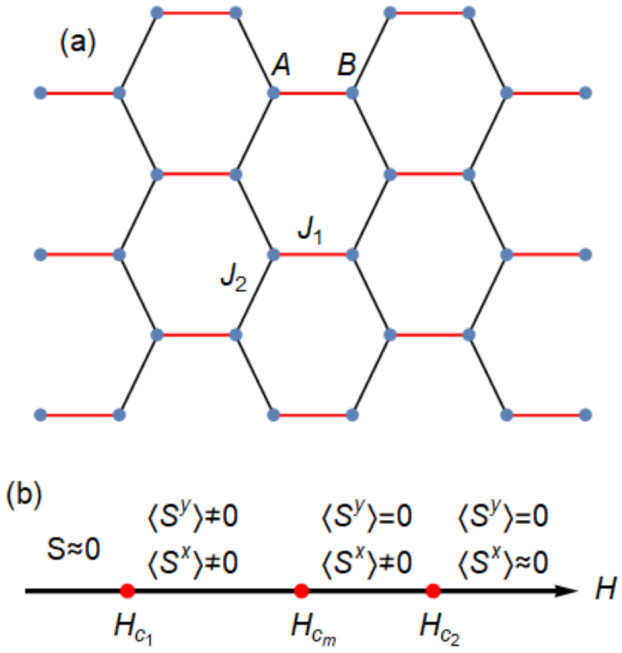

Figure 3.1: (a) A section of the honeycomb lattice. Each spin (blue dots) has a preferred neighbor (red bonds) which it interacts with more strongly than others: $J_1 > J_2$. For $h = 0$, the ground state is a product of singlets along the red bonds. (b) Schematic $T = 0$ phase diagram obtained from DMRG and mean-field theory. From left to right, the phases are a global spin singlet, $\mathbb{Z}_2$ symmetry breaking antiferromagnet, canted antiferromagnet, and the polarized phase. The critical points H_{c_1} and H_{c_m} are in the Ising universality class while H_{c_2} is a crossover.

As we will see, there is a regime of parameters which yields the phase diagram in Fig. 3.1(b). This phase diagram matches thermodynamic data by providing a mechanism for both breaking and restoring an Ising symmetry in spin-space as an external magnetic field is tuned. For $H_{c_1} < H < H_m$, the ground state breaks a $\mathbb{Z}_2$ symmetry in spin-space associated with the global transformation $S_i^y \to -S_i^y$, while for $H > H_m$ the system exhibits no symmetry breaking. Importantly, these effects are observable with weak anisotropy: we believe this can explain the coexistence of familiar and unfamiliar features observed in $Yb_2Si_2O_7$ [1].

We will use a variety of complementary techniques to develop a theory which accounts for the observations of $Yb_2Si_2O_7$. In order to motivate our model (3.1), we begin with a review of salient experimental facts. We then use a linked cluster expansion to compute the triplon spectrum and critical fields of the pure Heisenberg model, H_{c_1} and H_{c_2}. Our results are consistent with experimental findings and confirm that the (unperturbed) Heisenberg model captures important aspects of the physics of $Yb_2Si_2O_7$. Spin-wave theory is then applied to the full Hamiltonian (3.1) to show that the perturbations we have introduced produce dispersion relations which are qualitatively consistent with neutron scattering data. We emphasize that a complete microscopic theory supported by ab initio methods is necessary for complete quantitative agreement with empirical data. We then develop an understanding of the new order induced by these perturbations through a self-consistent mean field theory, which reveals the previously undetermined ground state order to be a canted antiferromagnet with a large staggered magnetic susceptibility and no broken symmetries. This physical picture is then quantitatively verified via a density matrix renormalization group (DMRG) analysis, and our concluding remarks suggest experimental tests of our proposal.

Plausible modifications to the Heisenberg model are strongly constrained by the available experimental data. To establish constraints on the parameters introduced in (3.1), we will now review the salient experimental results [1].

1. *Critical fields and zero-field specific heat are modeled well by the pure Heisenberg model.* In Ref. [1] , it was demonstrated that the Heisenberg model fits zero-field specific heat data.

We will also show that the Heisenberg model is consistent with the empirical values of H_{c_1} and H_{c_2}, which do not depend sensitively on weak perturbations.

2. *The XY antiferromagnet hosts an approximate Goldstone mode.* Within the energy resolution of available data, there is a gapless mode in the band structure of the planar antiferromagnet. This is presumably due to the presence of a proximate $U(1)$ spin-symmetry, which constrains the XY exchange anisotropy.

3. *Singularities in the specific heat present in weak fields vanish with increasing field.* In weak fields, an Ising-like singularity is observed as a function of temperature. Increasing the field to $H_m \approx 1.2$ Tesla removes the singularity and leads to smooth behavior as a function of temperature. Ultrasound velocity and neutron scattering measurements offer additional evidence of a phase transition at H_m.

Together, these points suggest that the Heisenberg model provides a strong basis for an analysis of $Yb_2Si_2O_7$. However, it is clear that the ground state breaks different (discrete) symmetries as a function of magnetic field, which is not a feature of the pure Heisenberg model. Moreover, the ground state for $H > H_m$ smoothly crosses over to the polarized limit at $H = H_{c_2}$.

3.2 Phenomenology of a Universal Spin Model

The perturbations to the Heisenberg model which we have introduced are designed to respect these experimental constraints while providing a mechanism for both breaking and restoring an Ising symmetry as a magnetic field is applied. The key changes are to the XY Heisenberg couplings, $J^y_{ij} = (1+\lambda)\, J^x_{ij}$, and a staggered g-tensor component $g_{zx} \ll g_{zz}$, $g^A_{zx} = -g^B_{zx}$. By choosing $\lambda \ll 1$, the first two experimental points are addressed: many qualitative features of the Heisenberg model are preserved and the Goldstone mode is only weakly gapped, potentially below empirical sensitivity. The staggered g-tensor creates a field-dependent competition between antiferromagnetic orders in the X-Y plane. For weak magnetic fields in the ordered phase ($H_{c_1} < H < H_m$), the YY coupling dominates, and the ground state breaks the $\mathbb{Z}_2$ spin symmetry

of the Hamiltonian. In larger magnetic fields ($H > H_m$), no symmetry is broken because the staggered g-tensor selects a unique antiferromagnetic order. In spin-wave theory, H_m corresponds to the magnetic field for which $\langle \mathbf{S}_y \rangle = 0$ everywhere. Since it breaks no symmetries, this state can cross over smoothly to the polarized limit ($H > H_{c_2}$).

We note that a staggered g-tensor is technically forbidden by the inversion symmetry of the C2/m crystal structure. However, weak deviations from this structure due to lattice distortions are not ruled out by available data. Such a distortion has clear experimental signatures, for example, by nuclear magnetic resonance (NMR) techniques. The required weakness of our staggered g-tensor element (see Fig. 3.8 and surrounding discussions) is consistent with a distortion-based explanation.

Further, we have explored similar models with uniform g-tensors and found that they do not reproduce the phase diagram of Fig. 3.1. Essentially, a uniform g-tensor does not lead to a field-dependent competition between antiferromagnetic orders: instead, spins simply have a polarization in the $x-z$ plane proportional to the effective field in each direction. While we have not completely ruled out the possibility that a model with inversion symmetry could produce the correct universal physics, we believe that no such model is consistent with the aforementioned experimental constraints.

The parameters we will choose throughout the following, unless otherwise noted, are $\lambda = 0.03$ and $g_{zx} = g_{zz}/100$. We take the x-component of the Heisenberg coupling to be the value obtained experimentally for the isotropic Heisenberg model, $J_1^x = 0.2173$ meV, $J_2^x = 0.0891$ meV. Conversions to physical magnetic fields are done with empirically determined g-factors [1]. We have found that our results do not qualitatively depend on these choices except in our DMRG analysis, where this issue is discussed in greater detail. Data on the effect of parameter choices at the mean-field level is also provided (see Figures 3.5 and 3.6).

3.2.1 Linked Cluster Expansion

Here we simplify to the isotropic Heisenberg model ($\lambda = 0$) and assume the z-axis is a principal axis of g ($g_{z\alpha} \propto \delta_{z\alpha}$). We will perturbatively compute the critical fields of the BEC transition and show that the result is consistent with experiments. In the limit $J_2 = h = 0$, the ground state of (3.1) is a collection of independent spin singlets. For finite J_2 with $J_2/J_1 \ll 1$, the ground state remains in the $S = 0$ sector with a gap to mobile triplet excitations. We compute the spectrum of these "single-particle" states with the linked cluster formalism. This yields a perturbative expression in J_2/J_1 which accurately describes the thermodynamic limit [71–73].

The resulting spectrum has a minimum at $\mathbf{k} = 0$, and we find that (defining $J_2/J_1 = \alpha$)

$$\omega\left(\mathbf{k}=0\right) = J_1\left(1-\alpha-\alpha^2+\frac{5}{16}\alpha^3+\mathcal{O}\left(\alpha^4\right)\right) \tag{3.2}$$

For $h \neq 0$, the $S^z = 1$ triplet band decreases linearly in energy leading to a gap closing. The resulting BEC transition has been studied extensively [83, 88–93]. Choosing the couplings and gyromagnetic factors reported in Ref. [1], we find the critical field $H_{c_1} \approx 0.434$ Tesla, in rough agreement with the experimental data. The upper critical field, H_{c_2}, of the Heisenberg model can be calculated exactly by considering the energetic cost of a spin flip in the polarized phase. We find $H_{c_2} = J_1 + 2J_2 \approx 1.42$ Tesla, also in agreement with experiment.

The singlet ansatz for the ground state is not correct in the presence of anisotropy when $h \neq 0$. However both mean-field and DMRG analyses indicate that the system becomes effectively paramagnetic below H_{c_1} in the presence of weak anisotropy (see figure 3.7). The agreement between these critical fields and the experimental results provides an *a-posteriori* justification for our focus on perturbative adjustments to the Heisenberg model.

3.2.2 Spin-Wave Theory

We now return to the full model (3.1). By introducing anisotropy to the Heisenberg couplings, we have broken the U(1) symmetry which is expected to provide the Goldstone mode of the ordered phase. We therefore anticipate that the spectrum is gapped, and the Goldstone mode observed

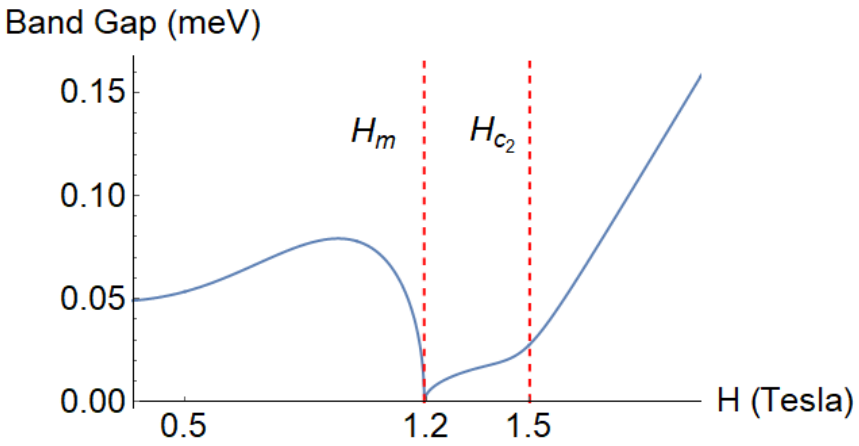

Figure 3.2: Band gap as a function of field in linear spin-wave theory. Other than the phase transition between spin wave solutions at $H = H_m$ (see text), the system is gapped with an energy scale near the energy resolution of available neutron scattering data. For $H > H_{c_2}$ the band gap scales linearly with H.

experimentally is in fact massive. Here we will use linear spin-wave theory to compute the spectrum and show that the resulting bands are qualitatively consistent with neutron scattering data.

Our ansatz for the classical spin orientations on sublattices A, B is for a canted antiferromagnet:

$$\begin{aligned} \mathbf{S}_A &= S\left(\sin\theta\cos\phi, \sin\theta\sin\phi, \cos\theta\right) \\ \mathbf{S}_B &= S\left(-\sin\theta\cos\phi, -\sin\theta\sin\phi, \cos\theta\right) \end{aligned} \tag{3.3}$$

Minimizing the Hamiltonian as a function of θ, ϕ yields two solutions. In weak fields,

$$\begin{aligned} \cos\theta &= \frac{h_z}{S\left(\bar{J}_z + \bar{J}_y\right)} \\ \cos\phi &= \frac{h_x\left(\bar{J}_z + \bar{J}_y\right)}{\left(\bar{J}_y - \bar{J}_x\right)\sqrt{S^2\left(\bar{J}_z + \bar{J}_y\right)^2 - h_z^2}} \end{aligned} \tag{3.4}$$

Here $\bar{J}_\alpha = J_1^\alpha + 2J_2^\alpha, h_z = g_{zz}h, h_x = g_{zx}h$. The critical field $H_m \approx 1.2$ Tesla is given by the condition $\cos\phi = 1$, and agrees with experimental data. For $H > H_m$ the system transitions to the solution

$$\phi = 0$$
$$\sin\theta = \frac{h_z \tan\theta - h_x}{S\left(\bar{J}_z + \bar{J}_x\right)} \tag{3.5}$$

Using the Holstein-Primakoff mapping to bosons (see details below), we obtain a quadratic Hamiltonian which can be diagonalized using standard techniques [16,94,95]. From the resulting dispersion, we extract the band gap as a function of the magnetic field (Fig. 3.2). The bands are gapped everywhere except at H_m, which separates the spin-wave solutions. The value of the gap exceeds experimental results, which not surprising in the absence of guidance from ab initio methods. However, key qualitative details which we expect are universal are captured, as we will now show.

The results presented above characterize the classical energetic minima for the canted antiferromagnet ansatz in terms of angles θ, ϕ. These define local sublattice-dependent coordinates in which $\hat{z}_i \propto \mathbf{S}_i$. We introduce sublattice-dependent rotation matrices $R(\theta,\phi)$ such that $\mathbf{S}_i = R^i(\theta,\phi)\tilde{\mathbf{S}}_i$, where $\tilde{\mathbf{S}}$ are the spins expressed in local coordinates. We then bosonize the spin model through the Holstein-Primakoff mapping,

$$\tilde{S}_i^z = S - a_i^\dagger a_i, \qquad \tilde{S}_i^+ = \sqrt{2S - a_i^\dagger a_i}\, a_i, \qquad \tilde{S}_i^- = a_i^\dagger \sqrt{2S - a_i^\dagger a_i} \tag{3.6}$$

To extract the band structure at leading order in $1/S$, it is sufficient to keep terms which are quadratic in boson operators. At this order, the Hamiltonian is expressed simply in terms of $\tilde{\mathbf{S}}$:

$$H_2 = \sum_{\langle ij\rangle} \sum_{\alpha,\beta=x,y,z} \left[A^{ij}_{\alpha\beta} \tilde{S}_i^\alpha \tilde{S}_j^\beta\right] - h\left(R^i_{zz} g_{zz} + R^i_{xz} g_{xz}\right) \sum_{i\in \mathrm{A}} \tilde{S}_i^z - h\left(R^j_{zz} g_{zz} - R^j_{xz} g_{xz}\right) \sum_{j\in \mathrm{B}} \tilde{S}_j^z \tag{3.7}$$

where A, B are the honeycomb sublattices and the parameters $A^{ij}_{\alpha\beta}$ are given by

$$A^{ij}_{\alpha\beta} = \sum_{\mu=x,y,z} J^{ij}_\mu R^i_{\mu\alpha} R^j_{\mu\beta} \tag{3.8}$$

At quadratic order in the boson operators, one may take $A_{zx} = A_{zy} = 0$. As a step to-

wards diagonalizing the boson Hamiltonian, we perform a Fourier transform which introduces the following parameters:

$$\tilde{A}_{\alpha\beta}(\mathbf{k}) = \sum_{j\in \mathrm{nn}(i)} A^{ij}_{\alpha\beta} \exp\left[i\mathbf{k}\cdot(\mathbf{r}_i - \mathbf{r}_j)\right] \tag{3.9}$$
$$\bar{A}_{\alpha\beta} = \sum_{j\in \mathrm{nn}(i)} A^{ij}_{\alpha\beta}$$

The final Hamiltonian is written compactly in terms of a vector of boson operators, with one boson flavor (a or b) per sublattice:

$$\Upsilon_{\mathbf{k}} = \left(a_{\mathbf{k}}\ b_{\mathbf{k}}\ a^{\dagger}_{-\mathbf{k}}\ b^{\dagger}_{-\mathbf{k}}\right)^{T}, \qquad H_2 = \sum_{\mathbf{k}} \Upsilon^{\dagger}_{\mathbf{k}} M(\mathbf{k}) \Upsilon_{\mathbf{k}} \equiv \sum_{\mathbf{k}} \Upsilon^{\dagger}_{\mathbf{k}} \begin{pmatrix} D(\mathbf{k}) & B(\mathbf{k}) \\ B^{\dagger}(\mathbf{k}) & D^{T}(-\mathbf{k}) \end{pmatrix} \Upsilon_{\mathbf{k}} \tag{3.10}$$

The matrices $D(\mathbf{k}), B(\mathbf{k})$ are given by

$$D(\mathbf{k}) = \begin{pmatrix} C(\mathbf{k}) & W^{*}(\mathbf{k}) \\ W(\mathbf{k}) & C(\mathbf{k}) \end{pmatrix}, \qquad B(\mathbf{k}) = \begin{pmatrix} 0 & X^{*}(\mathbf{k}) \\ X(\mathbf{k}) & 0 \end{pmatrix} \tag{3.11}$$

Where

$$\begin{aligned} C(\mathbf{k}) &= h\left(R^{i}_{zz} g_{zz} + R^{i}_{xz} g_{xz}\right) - S\bar{A}_{zz}(\mathbf{k}) \\ W(\mathbf{k}) &= \frac{S}{2}\left[\tilde{A}_{xx}(\mathbf{k}) + \tilde{A}_{yy}(\mathbf{k}) + i\left(\tilde{A}_{xy}(\mathbf{k}) - \tilde{A}_{yx}(\mathbf{k})\right)\right] \\ X(\mathbf{k}) &= \frac{S}{2}\left[\tilde{A}_{xx}(\mathbf{k}) - \tilde{A}_{yy}(\mathbf{k}) - i\left(\tilde{A}_{xy}(\mathbf{k}) + \tilde{A}_{yx}(\mathbf{k})\right)\right] \end{aligned} \tag{3.12}$$

Finally, the Hamiltonian (3.10) can be diagonalized by a Bogoliubov transformation. Cuts of the band structure are provided in Fig. 3.3 which are readily compared with the data shown in Fig. 4 of Ref. [1].

3.2.3 Mean Field Theory

In order to describe the novel phase observed in $Yb_2Si_2O_7$, we will now develop a qualitative understanding of the ground states of (3.1). We begin by formulating a mean-field theory using the

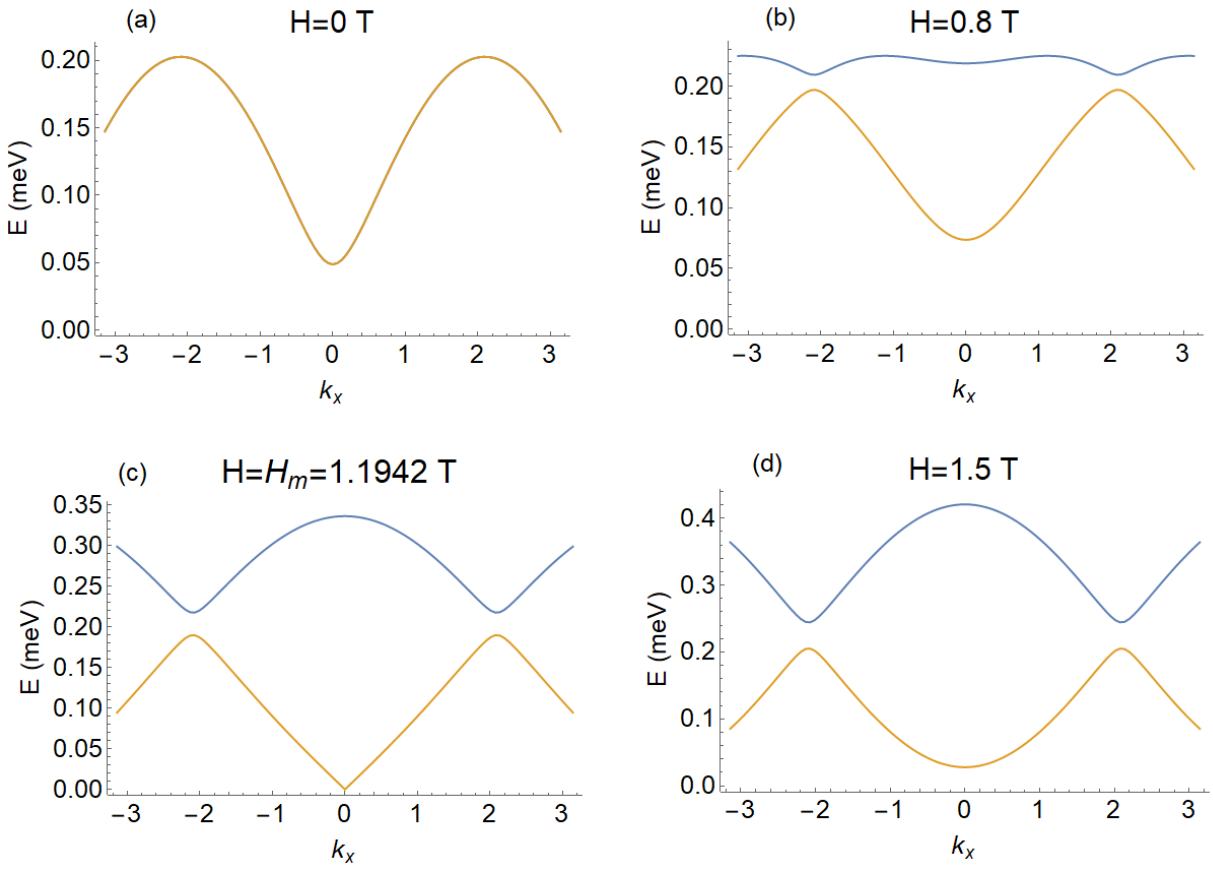

Figure 3.3: Cuts of the spin-wave spectrum ($k_y = 0$) for a range of magnetic fields. Between panels (b) and (c) ($H_{c_1} < H < H_m$), the concavity of the upper band changes, a feature which is also observed in neutron scattering data. At precisely $H = H_m$ (c), a linearly dispersing gapless mode appears at Γ. The bands scale linearly with H for $H > H_{c_2}$ (d).

bipartite structure of the honeycomb lattice and the fact that dimers are the relevant low-energy degrees of freedom. Let $\mathbf{M}_A, \mathbf{M}_B$ denote the average magnetic moments on sublattices A, B. The enhanced coupling J_1 between neighbors along $y = b$ suggests that the fundamental degree of freedom is a dimer containing spins $\mathbf{S}_A, \mathbf{S}_B$ embedded in an effective field. The Hamiltonian is

$$H = J_1^\alpha S_A^\alpha S_B^\alpha + 2J_2^\alpha \left(S_A^\alpha M_B^\alpha + S_B^\alpha M_A^\alpha\right) - h \sum_\alpha \left(g_{z\alpha}^A S_A^\alpha + g_{z\alpha}^B S_B^\alpha\right) \tag{3.13}$$

We assume $g_{zx} \ll g_{zz}$. The Hamiltonian (3.13) is analyzed self-consistently, starting with an ansatz for $\mathbf{M}_A, \mathbf{M}_B$ and calculating new values $\mathbf{M}_i \equiv \langle\psi|\mathbf{S}_i|\psi\rangle$, where $|\psi\rangle$ is the instantaneous ground state. These values are updated until convergence is achieved.

For sufficiently small g_{zx}, we find that the solution in Fig. 3.4 is energetically favored. For small fields ($H < H_{c_1}$), the solution is weakly magnetic due to the staggered field induced by g_{zx}. Between the critical fields $H_{c_1} < H < H_{c_2}$, two phases appear, distinguished by the staggered moment M_y. The first ($H < H_m$) exhibits $\mathbb{Z}_2$ symmetry breaking and accounts for the singularity observed in the specific heat; the latter breaks no symmetries and crosses over smoothly to the polarized limit, as required by the absence of thermodynamic singularities. This previously unidentified phase is a canted antiferromagnet with a strong staggered susceptibility.

We note the existence of another mean-field solution in which $M_y = 0$ everywhere. This case does not support the experimental data as it does not exhibit symmetry breaking. The energetic favorability of one mean-field solution over another depends on the precise anisotropy parameters chosen, and it is unclear how quantum fluctuations might impact that selection. Further, it is not obvious that the inter-dimer coupling J_2 is sufficiently small to justify a mean-field description. To address these concerns, we employ DMRG to investigate the stability of our results. By doing so, we find that both mean field solutions survive quantum fluctuations and remain energetically competitive. Further, there is a regime of parameters in which the solution in Fig. 3.4 is favored. Before introducing the DMRG results, we review the qualitative impact of our model parameter choices at the mean-field level in figures 3.5 and 3.6.

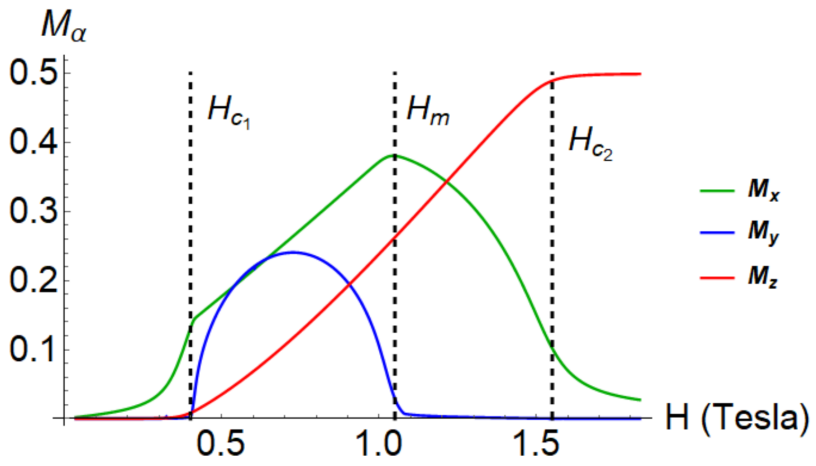

Figure 3.4: Spin expectation values as a function of magnetic field obtained from mean field theory ($\lambda = 0.03$, $g_{zx} = g_{zz}/100$). Note X and Y moments are staggered while Z is uniform. The presence of a nonzero M_y for $H_{c_1} < H < H_m$ indicates $\mathbb{Z}_2$ symmetry breaking and corresponds to the standard magnetic phase observed on the high-field side of the BEC phase transition without anisotropy. The range $H_m < H < H_{c_2}$ corresponds to a canted antiferromagnet which breaks no symmetries crosses over to the saturated regime at H_{c_2}.

The key parameters of our model Hamiltonian - namely the Heisenberg anisotropy λ and off-diagonal g-tensor element g_{zx} - can be adjusted to shift the locations of phase boundaries. Here we explore how the phase diagram is changed by such variations within dimer mean-field theory. We remind the reader that the effect of quantum fluctuations should always be considered before accepting mean-field results. However in our experience, the qualitative features of our mean-field theory are generally reliable.

The behavior of spin expectation values for different choices of λ are shown in Fig. 3.5. At $\lambda = 0$, no symmetry breaking is exhibited ($M_y = 0$). This is an exact statement, as the staggered g-tensor selects a unique planar order for all H. When $\lambda \neq 0$, there exists a range of magnetic fields in which symmetry breaking is energetically favored, and we see that $H_m \to H_{c_1}$ as $\lambda \to 0$. Larger values of λ favor symmetry breaking over a broader range of magnetic fields, sending $H_m \to H_{c_2}$. Returning to $\lambda = 0.03$, we now consider the effect of varying g_{zx} in Fig. 3.6. In this case, we see that sending $g_{zx} \to 0$ forces $H_m \to H_{c_2}$, and larger values of g_{zx} send $H_m \to H_{c_1}$.

The defining features of the "mystery" phase in our model ($H_m < H < H_{c_2}$) are the absence

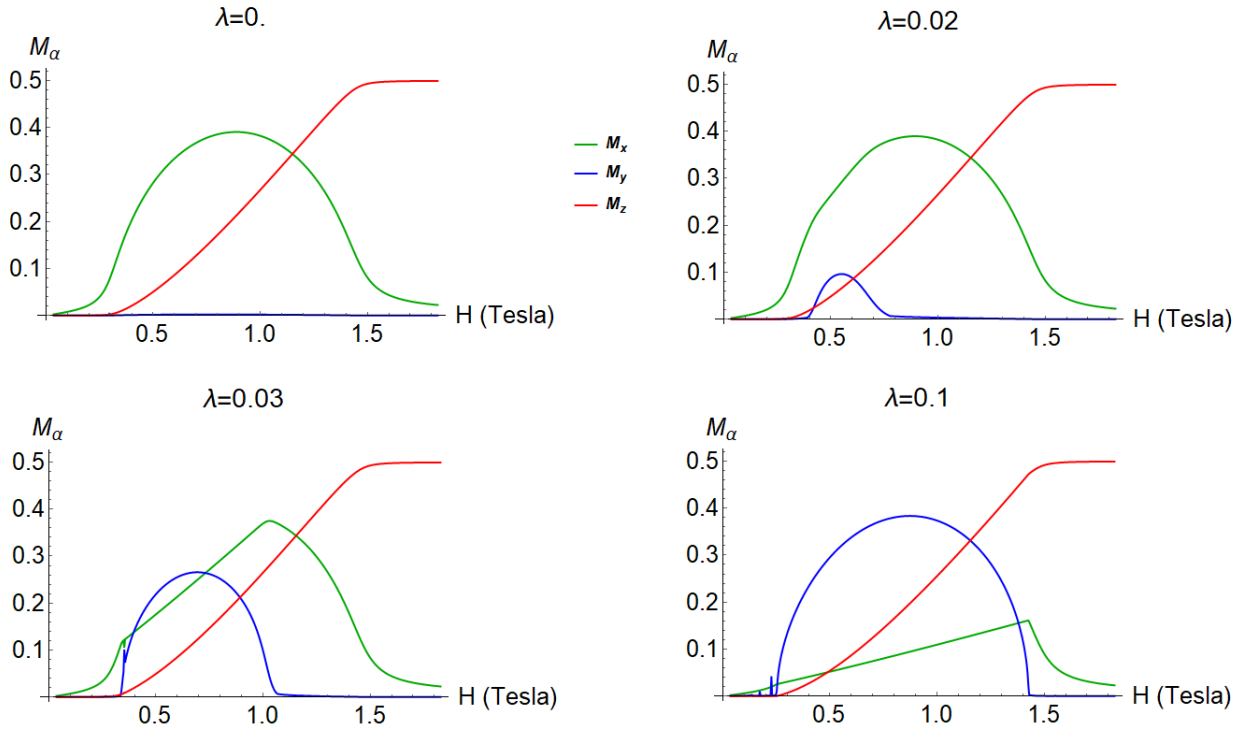

Figure 3.5: Spin expectation values for different choices of Heisenberg anisotropy λ. When $\lambda \to 0$, there is no energetic preference to break the $\mathbb{Z}_2$ symmetry discussed in the main text. For nonzero λ, symmetry breaking is energetically preferred for a range of magnetic fields, and shows that $H_m \to H_{c_1}$ as $\lambda \to 0$. As λ increases, $H_m \to H_{c_2}$, and the symmetry breaking regime dominates the phase diagram for $H_{c_1} < H < H_{c_2}$. We note that quantum corrections to our mean-field theory may shift these phase boundaries significantly.

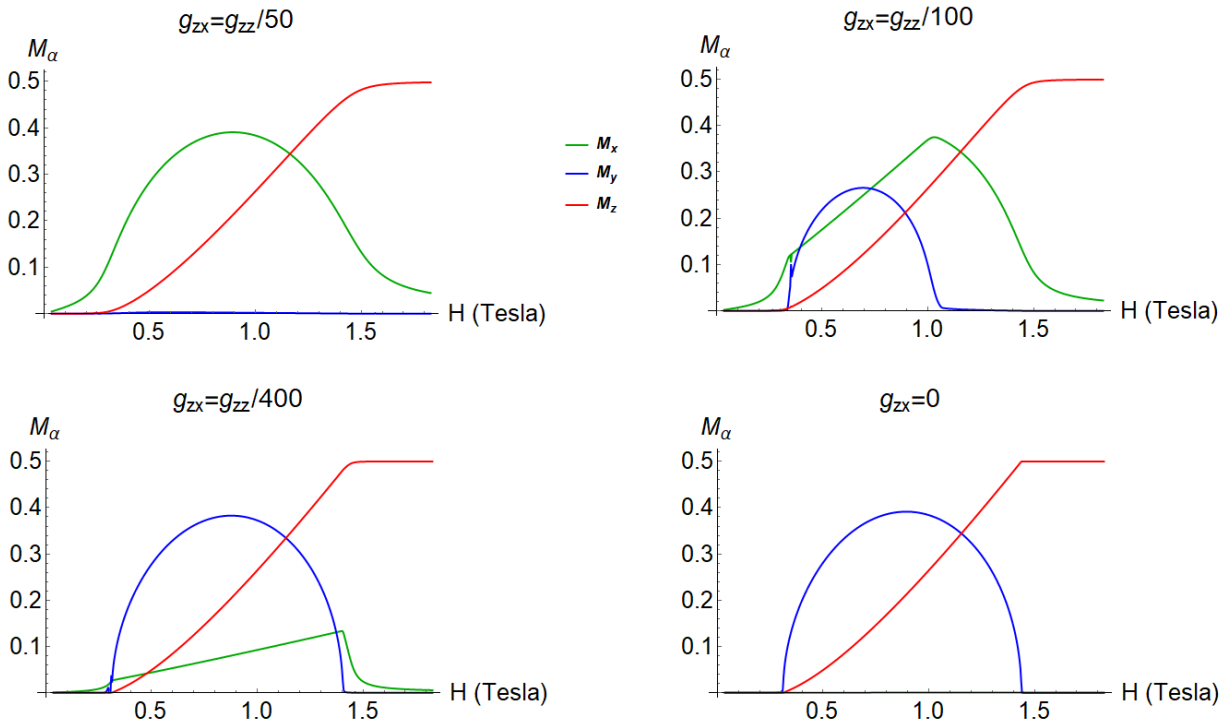

Figure 3.6: Spin expectation values for different choices of the g-tensor element g_{zx}. Large values of g_{zx} suppress symmetry-breaking by sending $H_m \to H_{c_1}$, while smaller values of g_{zx} favor symmetry breaking by sending $H_m \to H_{c_2}$.

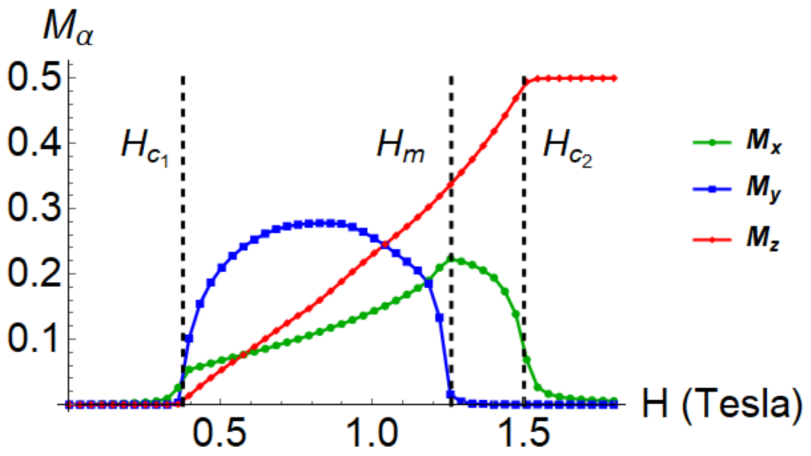

Figure 3.7: Spin expectation values as a function of magnetic field from DMRG ($\lambda = 0.03, g_{zx} = g_{zz}/500$). The qualitative agreement with Fig. 3.4 confirms that the universal physics obtained via mean-field theory is accurate. The data again indicates a field-driven phase transition from a broken symmetry state ($H_{c_1} < H < H_m$) to a state which breaks no symmetries ($H_m < H < H_{c_2}$).

of symmetry breaking and the presence of a large staggered susceptibility along the x-axis. Taken together, Figures 3.5 and 3.6 show that H_{c_1} and H_{c_2} are robust to changes in λ and g_{zx} when compared to H_m. Creating a phase diagram in which the symmetry breaking ($H_{c_1} < H < H_m$) and non-symmetry breaking ($H_m < H < H_{c_2}$) phases occupy significant portions of the phase diagram require a combined tuning of these interactions.

3.2.4 DMRG

To verify the mean-field solution, we use DMRG to compute ground state expectation values [96]. This tensor network method efficiently simulates systems which are well-described by the matrix product state (MPS) ansatz [97–101]. Our system is studied on a cylinder with a width of four dimers and 128 total spins.

We use a single-site representation of the tensor network to update each step [102] with the Hamiltonian (3.1). To guarantee that the proper symmetry sector is obtained, we apply pinning fields on the open boundaries of the system to break the $\mathbb{Z}_2$ symmetry of the Hamiltonian. The pinning field is removed after two DMRG sweeps, and we find that in the symmetry breaking region this produces a lower-energy state than unbiased DMRG.

From the resulting ground-state wavefunction, local measurements of quantities $M_\alpha = \sqrt{\sum_{i=1}^{N_s} \langle \hat{S}_i^\alpha \rangle^2}/N_s$ are performed. The results are shown in Fig. 3.7 and qualitatively match those from mean-field theory. The nonzero value of M_y for $H_{c_1} < H < H_m$ requires $\mathbb{Z}_2$ symmetry breaking. This symmetry is restored for $H > H_m$, allowing for a smooth crossover to the polarized limit at H_{c_2}. The regime $H_m < H < H_{c_2}$ is distinguished from the polarized limit both by the large staggered susceptibility of X-moments and the continued growth of the Z-magnetization. We will also see below that this behavior qualitatively reproduces ultrasound velocity data in every regime of magnetic fields (see figure 3.9).

The results in Fig. 3.7 are found with $g_{xz} = g_{zz}/500$. The ratio of g-tensor elements is arbitrary and can affect which mean field solution is obtained; to account for this, Fig. 3.8 shows the dependence of the symmetry-breaking order parameter M_y on g_{zx} in a fixed magnetic field. The solutions were found by first tuning to $H = 0.9$T with pinning fields. The pinning fields are then removed and g_{zx} is increased. The ground state changes from a Y-ordered antiferromagnet to a state where $M_y = 0$ as g_{zx} increases. The instability of the symmetry-breaking solution to anisotropy in the g-tensor reveals that g_{zx} is necessarily small. This is consistent with the fact that a nonzero g_{zx} requires deviations from the C2/m crystal structure currently proposed experimentally; such distortions are expected to be weak. The qualitative features of the phase diagram should be robust to other perturbations.

Another key piece of experimental data presented in Ref. [1] is the ultrasound velocity. In $Yb_2Si_2O_7$, this quantity is closely related to the scattering intensity of the (2,0,0) magnetic Bragg peak. In our model, this Bragg peak corresponds to the total magnetization of the system. In Fig. 3.9, we present our reproduction of the ultrasound velocity from DMRG. We simply calculate the square of the magnetization along the z-axis for a range of magnetic fields, and compute its derivative through finite-difference methods. Our results clearly capture the qualitative features presented in Ref. [1].

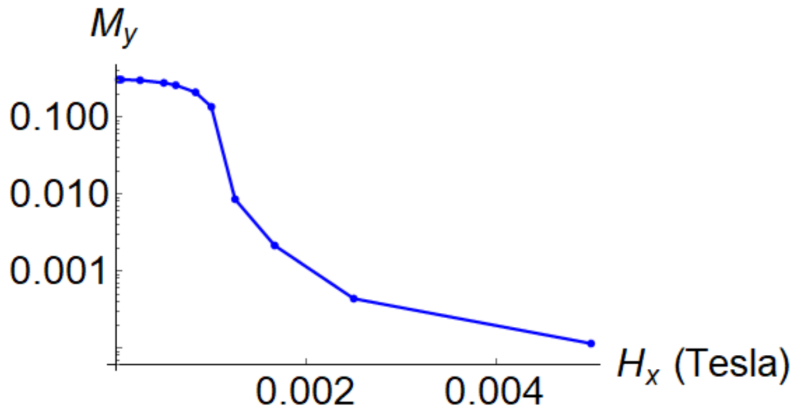

Figure 3.8: Dependence of M_y on the magnitude of the staggered field $H_x = g_{zx}H$ ($H = 0.9$T for each point). The value of M_y drops off rapidly with g_{zx}, indicating an instability of the symmetry-breaking mean-field solution to anisotropy in the g-tensor. Weakness of the anisotropy is therefore critical to the physics.

3.3 Conclusions

With a variety of theoretical techniques, we have demonstrated that the model (3.1) reproduces the experimentally proposed phase diagram of $Yb_2Si_2O_7$. These techniques complement each other; each of them supports the physical picture presented in this chapter. We emphasize again that weak perturbations to the Heisenberg model can explain the observed thermodynamic responses of Ytterbium Silicate, with an associated reduction of crystallographic symmetry.

Experimental verification of these details remains crucial, and our theory suggests natural tests of itself. The structure of local magnetic moments in the material can be probed with NMR techniques. In particular, observation of a staggered magnetization along a^* in the regime $H_m < H < H_{c_2}$ would confirm that a C2/m forbidden, staggered g-tensor is essential to describing $Yb_2Si_2O_7$. Further, more precise neutron scattering measurements may reveal a spin gap for $H_{c_1} < H < H_m$, the magnitude of which would constrain the XY anisotropy of our model.

Overall, this example illustrates how perturbations such as spin-orbit coupling can be used to induce effective interactions that lead to non-trivial magnetic orders. Future studies focused on the continuum theory of this model would also be interesting as a variation on the broader theme of Bose-Einstein condensation in magnets.

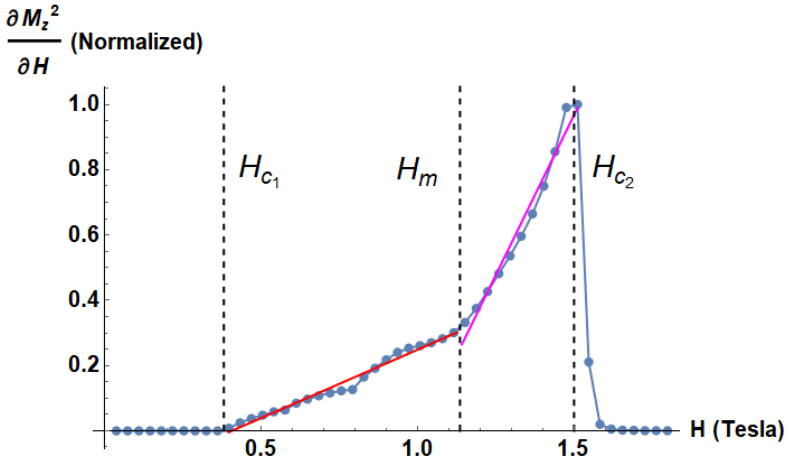

Figure 3.9: Derivative of the scattering intensity $I \propto M_z^2$ with respect to a magnetic field H, obtained by DMRG. Linear fits to the data are shown for the regimes $H_{c_1} < H < H_m$ (red) and $H_m < H < H_{c_2}$ (magenta); the scaling of dI/dH clearly changes in these regimes. The qualitative behavior of our results compares favorably with the data of Ref. [1], see Fig. 3(c). We have normalized our data such that the peak at H_{c_2} is equal to 1.

Chapter 4

The Distorted Pyrochlore Heisenberg Model [1]

4.1 Motivation & Definition of The Model

This chapter focuses on a classical model of Heisenberg spins on the sites of the pyrochlore lattice, a non-Bravais lattice with a four-site basis. Spins in this basis occupy the vertices of a tetrahedron, so that the full lattice is built out of vertex-sharing tetrahedra (see figures 4.1 and 4.2). The triangular motifs that compose these tetrahedra are responsible for an extraordinary degree of geometric frustration, leading to the famous prediction that the nearest-neighbor Heisenberg antiferromagnet on the pyrochlore lattice is a classical spin liquid [103]. By this, we mean that even at arbitrarily low temperatures, any correlation function is disordered in the sense that its average over the set of ground states decays exponentially. This remarkable behavior leads to the breakdown of standard mean-field approaches, including spin-wave theory and large-N calculations with Schwinger bosons [104, 105]. For these reasons, the pyrochlore Heisenberg model has inspired an impressive range of studies which often pioneer novel methods in many-body theory.

Along any <111> axis, the pyrochlore lattice can be viewed as alternating layers of kagomé and (sparse) triangular lattice structures (see Figure 4.3). Like the pyrochlore lattice, the kagomé lattice (figure 1.1) is highly frustrated: it retains all of the pyrochlore's triangular plaquettes

[1] The contents of this chapter are currently unpublished. The author anticipates publication of this work with Rajiv R.P. Singh and T.E. Baker.

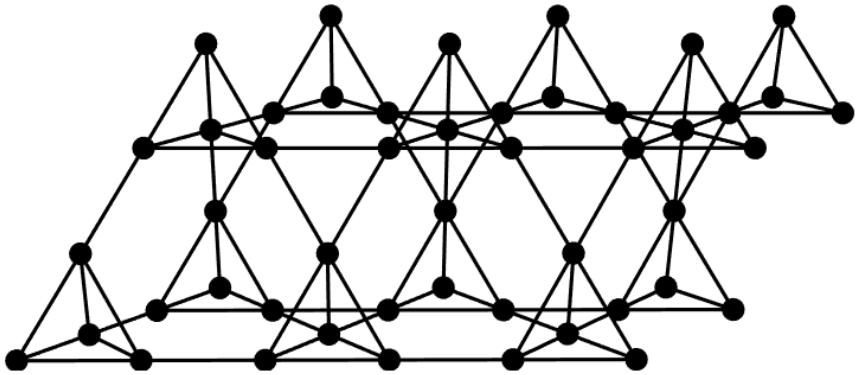

Figure 4.1: A section of the pyrochlore lattice, built out of twelve unit cells of upward facing tetrahedra.

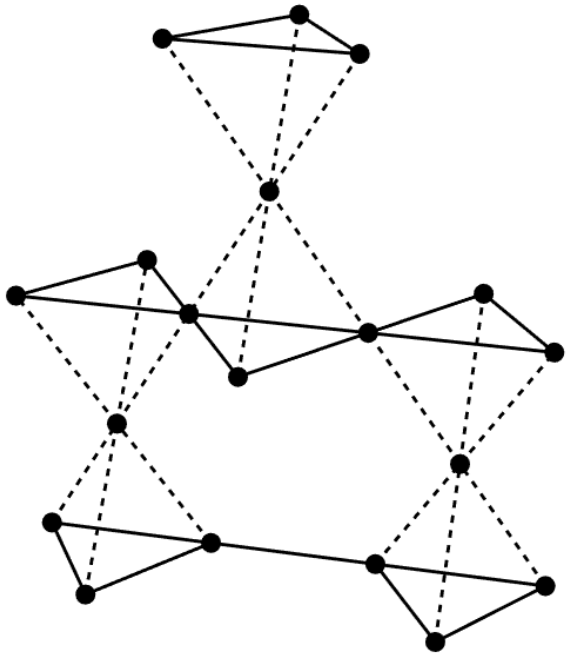

Figure 4.2: A small section of the pyrochlore lattice, with an illustration of the geometric distortion in (4.1). Solid lines represent Heisenberg exchange with coupling J, while dashed lines represent weakened exchange λJ. Three-dimensional "bowtie" structures centered on triangular-lattice spins are natural fundamental units in this problem.

present in a commensurate planar cut. However, the nearest neighbor Heisenberg antiferromagnet is *not* a classical spin liquid on the kagomé lattice [106]. At low temperatures, the kagomé model is known to exhibit a subtle ordering mechanism. This mechanism, dubbed order-by-disorder, counterintuitively relies on thermal (or quantum) fluctuations to establish long-range order [107–110]. We will review this carefully in section 4.2; for now, we note that this phenomenon results in the entropic selection of co-planar ground state configurations at nonzero temperatures [111]. This implies that the low-temperature limit of the kagomé Heisenberg model has non-trivial nematic correlation functions.

The stark contrast in low temperature behavior between kagomé and pyrochlore antiferromagnets raises natural questions for pyrochlore materials. In particular, how is the order-by-disorder mechanism of individual kagomé layers lost in the pyrochlore lattice? Our goal in this chapter is to answer this question. We approach the problem by considering a model Hamiltonian which continuously interpolates between the Heisenberg model on decoupled kagomé sheets ($\lambda = 0$) and the undistorted pyrochlore lattice ($\lambda = 1$) (see Figure 4.2 for an illustration of the couplings):

$$H = J \sum_{\langle ij \rangle \in \text{kag}} \mathbf{S}_i \cdot \mathbf{S}_j + \lambda J \sum_{\langle ij \rangle \notin \text{kag}} \mathbf{S}_i \cdot \mathbf{S}_j \tag{4.1}$$

where the summations are over bonds contained within kagomé layers and external to them, respectively. After reviewing the phenomena of order-by-disorder in the kagomé Heisenberg model, we will characterize the ground states of (4.1). In the process, we will show that there is a critical value of the geometric distortion, λ_c, below which there is a quasi-two dimensional regime that exhibits the order-by-disorder mechanism. For distortions in the range $0 < \lambda < \lambda_c$, we will also argue that the model exhibits a thermal crossover into a classical spin liquid phase as the temperature is reduced. We will comment throughout on the expected behavior of thermodynamic response functions, such as the specific heat.

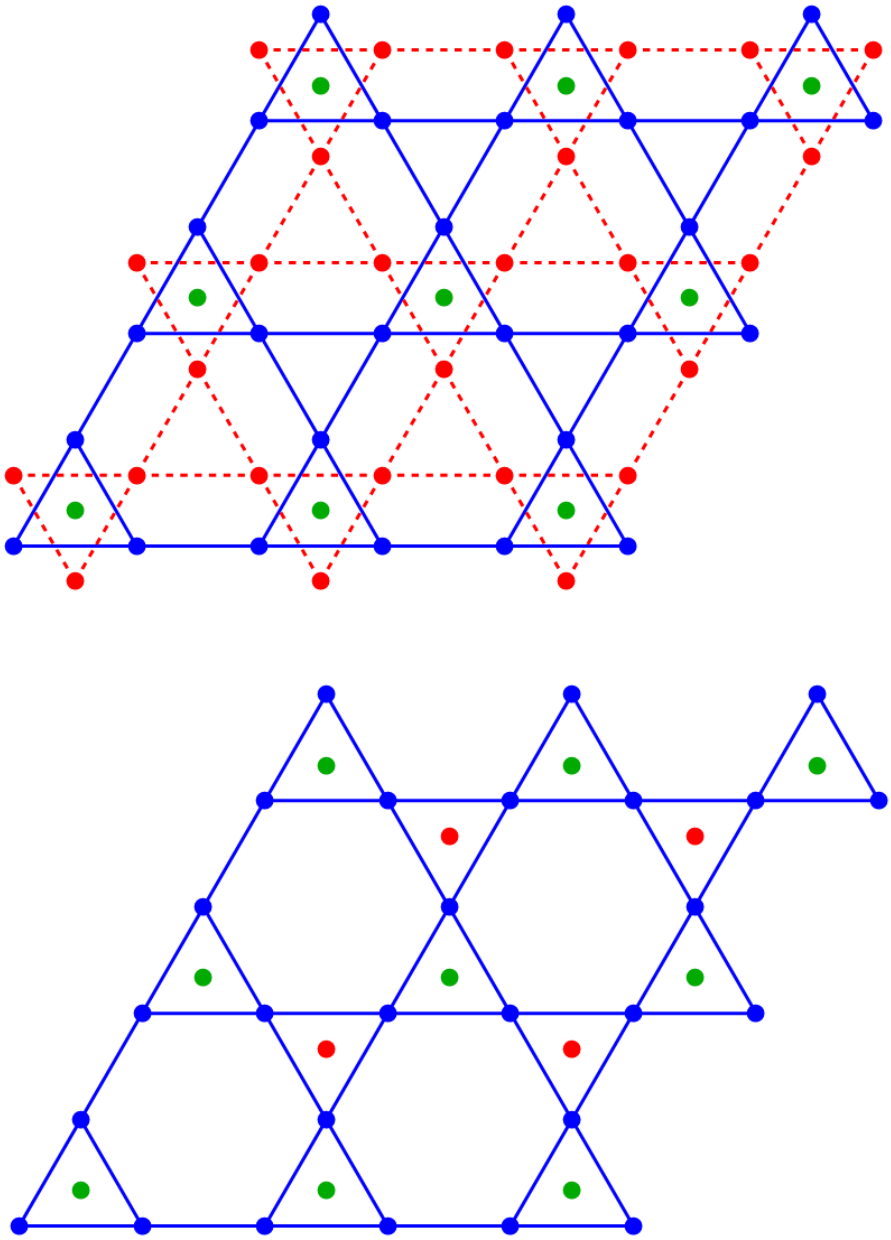

Figure 4.3: Cuts of the pyrochlore lattice along a <111> direction. Top: a triangular lattice layer (green) sandwiched between two kagomé layers (blue, red). Bottom: a kagomé layer (blue) sandwiched between two triangular lattice layers (green, red). In both cases, bonds within kagomé planes are shown. Bonds connecting kagomé and triangular lattice spins are ommitted for visualization.

4.2 Order-by-disorder and the kagomé Heisenberg Model

It is generally understood that fluctuations, either of a quantum mechanical or thermal nature, act to destroy order in many-body systems. In the context of classical statistical mechanics, this intuition essentially follows from the thermal behavior of Boltzmann weights. This perspective is also supported by paradigm-defining lattice systems, such as the two-dimensional Ising model, whose order parameter decays monotonically with increasing temperature. After working with standard solvable models, it might seem inconceivable that fluctuations are capable of inducing order.

On the other hand, we are taught in statistical mechanics that systems in thermal equilibrium select microstates which minimize the free energy $F = E - TS$. When considering the low-temperature physics of a lattice model, we often neglect the role of the entropy in determining the free energy. This is certainly reasonable for systems built out of discrete degrees of freedom with small ground state degeneracies. However, in systems with continuous degrees of freedom, such as Heisenberg spins, this issue becomes far more delicate due to the presence of continuous, zero-energy distortions of many-body states. When these continuous degrees of freedom are combined with a large ground state degeneracy due to frustration, it is clear that entropic effects cannot be ignored: fluctuations may lift the ground state degeneracy and induce a systematic preference for a particular subset of the ground states.

A general framework for understanding the role of fluctuations in thermodynamic selection was put forward by Moessner and Chalker, which we review here [103,112]. Let $\mathbf{x}$ be a coordinate in many-body configuration space which parameterizes the ground state manifold (for all cases considered in this chapter, this manifold is connected). If $\mathbf{y}$ parameterizes the distortions around this manifold due to fluctuations, the low-temperature effective Hamiltonian can be expressed in the form

$$H = \sum_{\ell} \epsilon_{\ell}(\mathbf{x})\, y_{\ell}^2 + \mathcal{O}\left(y_{\ell}^4\right) \tag{4.2}$$

where ℓ runs over the dimensionality of $\mathbf{y}$ and $\epsilon_{\ell}(\mathbf{x})$ is the harmonic cost of fluctuations at the ground state labeled by $\mathbf{x}$. Integrating over the fluctuations about the ground state at $\mathbf{x}$ gives a ground state probability distribution of the form

$$Z(\mathbf{x}) = \int d\mathbf{y} e^{-\beta H} \propto \prod_{\ell} \sqrt{\frac{k_B T}{\epsilon_{\ell}(\mathbf{x})}} \tag{4.3}$$

It may be the case that harmonic terms happen to vanish for specific ground states. If this produces a non-integrable singularity in (4.3), order-by-disorder occurs as almost all statistical weight is concentrated on this ill-behaved subset. By keeping higher-order terms in (4.2), a well-defined expression for $Z(\mathbf{x})$ follows. Moreover, equipartition directly relates the specific heat to the scaling behavior of fluctuations about the selected subspace.

For these reasons, we anticipate that the ground states with the largest number of anharmonic (or "soft") modes will be selected for $T > 0$. If this subset of ground states has distinct symmetry properties from the set of all ground states, we conclude that introducing a small amount of disorder can actually induce order - hence the term order-by-disorder. This can also be understood as a discontinuity in the limiting behavior of the partition function:

$$\lim_{T \to 0} Z(T) \neq Z(T = 0) \tag{4.4}$$

This is precisely the qualitative behavior observed in the classical nearest-neighbor kagomé antiferromagnet. The Hamiltonian of this model can be written as

$$H = J \sum_{\langle ij \rangle} \mathbf{S}_i \cdot \mathbf{S}_j = \frac{J}{2} \sum_{\Delta} \left(\mathbf{S}_{\Delta}^2 - 3\right) \tag{4.5}$$

where the last expression is a sum over all kagomé triangles. The ground states of (4.5) satisfy $\mathbf{S}_{\Delta}^2 = 0$ on every plaquette. The number of ground states grows exponentially as a function of system size, and at zero temperature each one contributes equally to computations of correlation

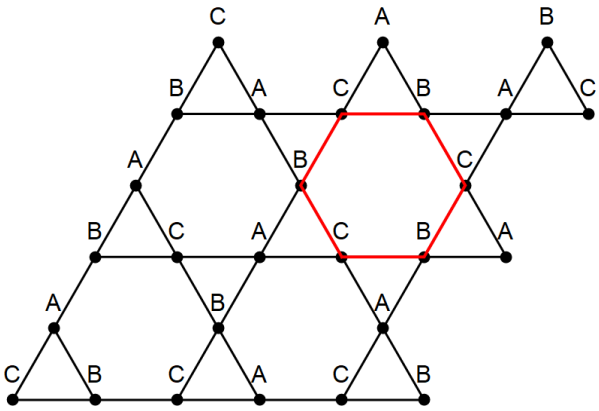

Figure 4.4: An example of a co-planar state on the kagomé lattice. Spins can be in one of three configurations (labeled A, B, C) in a co-planar state. A gapless "weathervane defect" is highlighted in red. Closed curves built out of two spin states can be rotated with zero energetic cost about the axis of the third spin state, leading to selection of co-planar states.

functions [113].

At small but nonzero temperatures, thermal fluctuations appear. What ground states could they prefer? A natural subspace to consider, due to their unique geometric properties, is the set of co-planar ground states. These are ground states in which every spin lies in the same plane as every other; combined with the local ground state constraint $\mathbf{S}_\Delta^2 = 0$, this implies that every spin can point in one of three directions (see Figure 4.4). These directions are related by $2\pi/3$ rotations about the axis normal to the ordering plane. Co-planar ordering implies that nematic long-range correlation functions will be nonzero, since the normal vector to the spin plane of each kagomé triangle will either be parallel or antiparallel to any other.

The important properties of fluctuations about a co-planar state can be understood by studying a single plaquette. For a kagomé triangle, a ground state configuration is given by

$$\mathbf{S}_j = \left(\cos\left(2\pi j/3\right), \sin\left(2\pi j/3\right), 0\right), \quad j = 1, 2, 3 \tag{4.6}$$

Now study fluctuations normal to the spin plane by fixing $\mathbf{S}_1$ and allowing variations of the form

$$\mathbf{S}_2' = \mathbf{S}_2 + (0, 0, \eta) \tag{4.7}$$
$$\mathbf{S}_3' = \mathbf{S}_3 - (0, 0, \eta)$$

One can then check that the change in energy due to these fluctuations scales as η^4; note the absence of a harmonic term. More generally, the fluctuations (4.7) can be understood as rotations of the vectors $\mathbf{S}_2, \mathbf{S}_3$ about the axis defined by $\mathbf{S}_1$. It is this interpretation of the normal fluctuations which extends to the many-body co-planar state, and leads to their selection.

More explicitly, consider an arbitrary co-planar ground state, and label the three distinct spin orientations A, B, C (see Figure 4.4). Any curve on the lattice - open or closed - built out of only, for example, A and B spins is associated with a quartic mode generated by rotations about the C-axis. Remarkably, it has been shown via spin-wave theory that every co-planar state has a number of quartic modes equal to the number of hexagons on the lattice. These "weathervane defects" may be spatially local (i.e., on closed curves, as in Figure 4.4) or extend to infinity on open curves in the thermodynamic limit. Moreover, it has been proven that any non-coplanar state has fewer quartic modes than the co-planar states. For this reason, fluctuations in the low-temperature limit select co-planar ground state configurations.

This result has immediate consequences for thermodynamic properties, particularly the specific heat. Let N_h be the number of hexagons on the lattice (with periodic boundary conditions) and N_s be the number of spins. Then $N_s = 3N_h$, and by equipartition, we find

$$C = k_B \left(N_s - N_h/4\right) = \frac{11}{12} N_s k_B \tag{4.8}$$

This prediction has been verified by numerical simulations, and confirms that the low-temperature statistical weight of fluctuations is overwhelmingly concentrated on co-planar ground states.

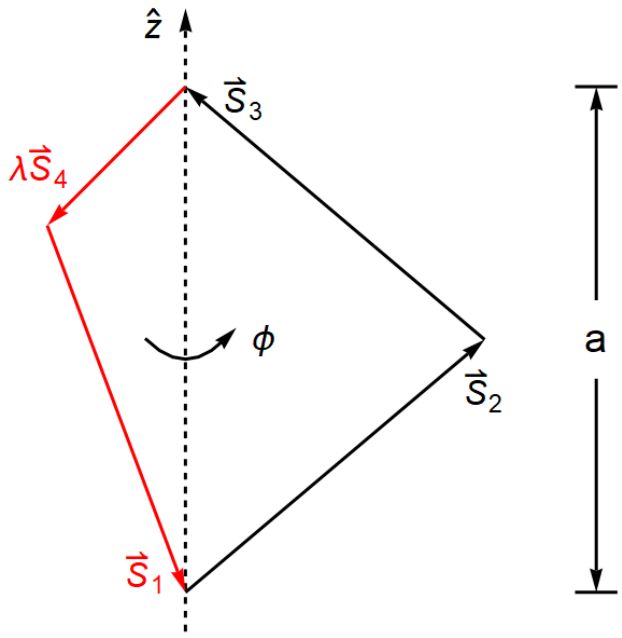

Figure 4.5: Geometric parameterization of single-tetrahedron ground states. The case shown assumes $\lambda = 1/2$, but its qualitative features are generic. The continuous variables a, ϕ completely parameterize the ground state manifold for a single tetrahedron, and can always be chosen independently for $\lambda < 1$.

4.3 Isolated Tetrahedra

We now return to the distorted pyrochlore Heisenberg model, focusing initially on individual tetrahedra (or pairs of tetrahedra). While some relevant many-body phenomena cannot be observed in this context, studying a single tetrahedron is sufficient to determine the local constraints satisfied by all many-body ground states. We will also derive an effective Hamiltonian which demonstrates the emergence of a quasi-two dimensional regime.

4.3.1 Ground States

The Hamiltonian (4.1), restricted to a single tetrahedron, is

$$\begin{aligned} H =& J\left(\mathbf{S}_1 \cdot \mathbf{S}_2 + \mathbf{S}_1 \cdot \mathbf{S}_3 + \mathbf{S}_2 \cdot \mathbf{S}_3\right) + \lambda J\left(\mathbf{S}_1 + \mathbf{S}_2 + \mathbf{S}_3\right) \cdot \mathbf{S}_4 \\ =& \frac{J}{2}\left(\mathbf{S}_\Delta^2 - 3\right) + \lambda J \mathbf{S}_\Delta \cdot \mathbf{S}_4 \end{aligned} \tag{4.9}$$

In the last line, we defined $\mathbf{S}_\Delta \equiv \mathbf{S}_1 + \mathbf{S}_2 + \mathbf{S}_3$ and used the fact that $|\mathbf{S}_i| = 1$. In this section, we will retain constant shifts to the Hamiltonian for the sake of clarity, but we will neglect them in general. By varying the magnitude $|\mathbf{S}_\Delta|$, one can show that ground states of (4.9) satisfy

$$\mathbf{S}_\Delta = -\lambda \mathbf{S}_4 \tag{4.10}$$

This result extends beyond isolated tetrahedra: ground states of the full Hamiltonian (4.1) are those which satisfy the constraint (4.10) for every tetrahedron. The ground state energy for these configurations (per tetrahedron) is found to be

$$E_{\text{gs}} = -\frac{J}{2}\left(3 + \lambda^2\right) \tag{4.11}$$

We can see that the geometric distortion has introduced a new energy scale, $\lambda^2 J$. It is already clear at this stage that this energy scale must be closely related to the thermal transition between quasi-two dimensional and three dimensional behavior mentioned previously. This scaling will be shown to persist following more careful considerations for many-body ground states.

Going forward, it will be useful to have an explicit geometric parameterization of these ground state configurations on each tetrahedron. This problem was solved by Moessner and Chalker in the case $\lambda = 1$ [112]. Here we will provide a simple generalization to $0 < \lambda \leq 1$.

By absorbing λ into $\mathbf{S}_4$, the constraint (4.10) can be restated as the requirement that three vectors of unit length and one of length λ must sum to zero (see figure 4.5). Begin by considering spins $\mathbf{S}_4$ and $\mathbf{S}_1$. Without loss of generality, we can choose coordinates such that their sum lies along a Cartesian direction: $\mathbf{S}_1 + \lambda \mathbf{S}_4 = a\hat{z}, 1 - \lambda \leq |a| \leq 1 + \lambda$. Now consider the spins $\mathbf{S}_2, \mathbf{S}_3$. Without loss of generality, we can select the plane in which they order, which we parameterize by an angle ϕ relative to the $\mathbf{S}_1, \mathbf{S}_4$ plane. To satisfy (4.10), it must be the case that $S_2^z = S_3^z = -a/2$, which uniquely fixes the configurations of $\mathbf{S}_2$ and $\mathbf{S}_3$ in the plane determined by ϕ. The ground state manifold for a single tetrahedron is therefore completely parameterized by the variables a, ϕ. In section 4.4.1, we will use this parameterization to argue that the many-body ground state manifold contains no energy barriers - any ground state can be continuously deformed into any

other without energetic cost.

Some consequences immediately follow for $\lambda < 1$. It was noted by Moessner and Chalker that a special subset of ground states in the $\lambda = 1$ case are the collinear states, in which each tetrahedron is divided into pairs of antiparallel spins (corresponding to $a = 0$ or $\phi = \pi$). These cases are pathological in the sense that the parameters a and ϕ cannot be chosen independently; the fact that collinear states are not ground states for $\lambda \neq 1$ guarantees that the parameters a and ϕ can always be chosen independently.

We will be particularly interested in the behavior of ground states for small values of λ, for which thermal fluctuations are found to play a significant role. When $\lambda \ll 1$, the spins $\mathbf{S}_1, \mathbf{S}_2$, and $\mathbf{S}_3$ will be approximately coplanar, in the sense that $|\mathbf{S}_1 + \mathbf{S}_2 + \mathbf{S}_3| \sim \mathcal{O}(\lambda^2)$.

4.3.2 Effective Hamiltonian: kagomé layers

In anticipation of our interest in the regime $\lambda \ll 1$, this section will be used to derive an effective Hamiltonian by integrating out the weakly coupled spins on triangular lattice sites. We begin by considering a pair of tetrahedra with a common triangular lattice spin. We will call these "bowtie" structures for obvious reasons. Labeling the sum of moments in each kagomé triangle by $\mathbf{S}_{\Delta_1}$ and $\mathbf{S}_{\Delta_2}$, and the triangular lattice spin by $\mathbf{S}_t$, the Hamiltonian in this case can be written as

$$H = \frac{J}{2}\left(\mathbf{S}_{\Delta_1}^2 + \mathbf{S}_{\Delta_2}^2\right) + \lambda J \mathbf{S}_t \cdot \left(\mathbf{S}_{\Delta_1} + \mathbf{S}_{\Delta_2}\right) \tag{4.12}$$

An effective Hamiltonian H_{eff} is then obtained by integrating out $\mathbf{S}_t$:

$$\exp\left[-\beta H_{\text{eff}}\right] \equiv \int d\mathbf{S}_t \exp\left[-\beta H\right],$$

$$H_{\text{eff}} = \frac{J}{2}\left(\mathbf{S}_{\Delta_1}^2 + \mathbf{S}_{\Delta_2}^2\right) - \frac{1}{\beta}\ln\left[\frac{\sinh\left(\beta\lambda J|\mathbf{S}_{\Delta_1} + \mathbf{S}_{\Delta_2}|\right)}{\beta\lambda J|\mathbf{S}_{\Delta_1} + \mathbf{S}_{\Delta_2}|}\right] \tag{4.13}$$

with $\beta \equiv (k_B T)^{-1}$. We can see that integrating out $\mathbf{S}_t$ produces an effective ferromagnetic interaction between kagomé moments on opposite ends of bowtie structures, which is consistent with the constraint (4.10). A particularly important feature of H_{eff} is its explicit dependence on

temperature, which we will show leads to a thermal crossover between quasi-two dimensional and three dimensional behavior.

On symmetry grounds, we anticipate the ground states of (4.13) take the form $\mathbf{S}_{\Delta_1} = \mathbf{S}_{\Delta_2} \equiv S\hat{n}$, where the unit vector $\hat{n}$ is arbitrary. The energy of such a configuration is

$$E(S,\beta) = \frac{1}{2}JS^2 - \frac{1}{\beta}\ln\left[\frac{\sinh(2\beta\lambda JS)}{2\beta\lambda JS}\right] \tag{4.14}$$

Extremizing the energy over S leads to the transcendental equation

$$2JS + \frac{1}{\beta S} - 2J\lambda\coth(2\beta\lambda JS) = 0 \tag{4.15}$$

Generically, we can only solve (4.15) for the kagomé moment S numerically. However, the high and low temperature limits can be solved exactly by first order series expansion, with the result

$$\begin{aligned} S(\beta\to\infty) &= \lambda \\ S(\beta\to 0) &= 0 \end{aligned} \tag{4.16}$$

The zero-temperature limit is in agreement with the ground state constraints, while the infinite-temperature limit represents the anticipated quasi-two dimensional regime. Indeed, states with $S = 0$ correspond precisely to ground states of the Heisenberg model on decoupled kagomé sheets. Importantly, the quasi-two dimensional solution persists down to the thermal scale $k_BT \sim \alpha^2 J$. Assuming that S grows continuously as the temperature decreases (i.e., there is no first order transition), a series expansion of (4.15) in powers of S is justified, and a nonzero solution only appears when

$$\beta > \frac{3}{2J\lambda^2} \tag{4.17}$$

With this understanding of individual tetrahedra, we now move on to consider many-body ground states. In the following, we will see that the quasi-two dimensional regime is dominated

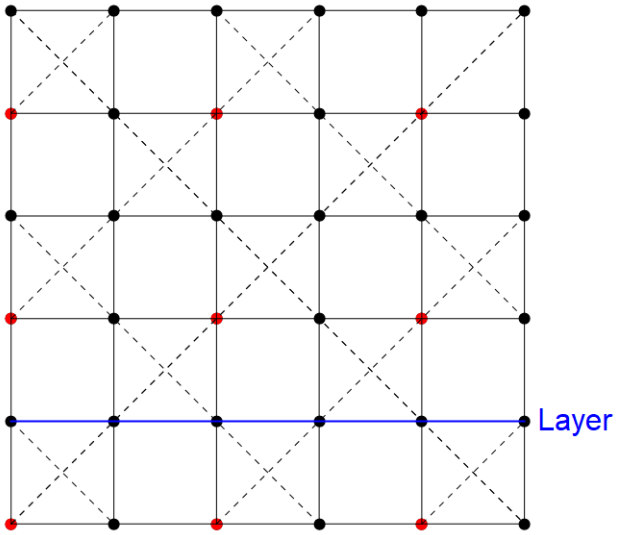

Figure 4.6: The square lattice with crossings. This lattice is fundamentally equivalent to the pyrochlore, but easier to visualize. Solid and dashed lines correspond to exchange interactions between spins. Spins colored red correspond to the apex of pyrochlore tetrahedra, so that every exchange interaction with a red vertex has strength λJ. An example of a layer used in our proof is highlighted in blue.

by the same fluctuations that control the low-temperature behavior of the kagomé Heisenberg model. We will also argue that there is no entropic selection at sufficiently low temperatures.

4.4 Many-body Results

We now consider the many-body problem of the distorted pyrochlore Heisenberg model. Our analysis will be motivated by insights obtained in the previous section for individual tetrahedra, and our understanding of the order-by-disorder mechanism for decoupled kagomé sheets.

4.4.1 Absence of Energy Barriers Between Ground States

All remarks in this section assume that we are dealing with a system that has open boundary conditions.

Moessner and Chalker have demonstrated previously that the ground state manifold of (4.1) is connected for the special case $\lambda = 1$ [112]. Their argument essentially carries over to the case $0 < \lambda < 1$, with some modifications that account for the absence of collinear ground states.

Following them, our approach to the proof is to argue that, for fixed λ, any ground state can be continuously deformed into a particular reference state without encountering energy barriers. Our reference state is a $q = 0$ state, for which the magnetic unit cell is a single tetrahedron. Using the notation of (4.9) and figure 4.5, our reference state of choice is one in which the spins $\mathbf{S}_3, \mathbf{S}_4$ are antiparallel. Using global spin-rotation symmetry, such a state can be written as (for fixed λ)

$$\begin{aligned}
\mathbf{S}_4 &= (0, 0, 1) \\
\mathbf{S}_3 &= (0, 0, -1) \\
\mathbf{S}_2 &= \left(\sqrt{1 - \frac{(1-\lambda)^2}{4}}, 0, \frac{1-\lambda}{2} \right) \\
\mathbf{S}_1 &= \left(-\sqrt{1 - \frac{(1-\lambda)^2}{4}}, 0, \frac{1-\lambda}{2} \right)
\end{aligned} \tag{4.18}$$

This configuration satisfies (4.10) on every tetrahedron in a $q = 0$ arrangement, and is in a sense the closest we can get to a collinear ground state for $\lambda < 1$. It is also useful to note for purposes of visualization that the pyrochlore is closely related to the square lattice with crossings, illustrated in Figure 4.6. Our approach to the proof will be to go through this lattice, layer by layer, and adjust spin configurations without returning to a previously visited layer. As we will see, this is possible for the square lattice with crossings, and for essentially identical reasoning applies to the pyrochlore lattice.

The proof will make use of the following facts.

1. On a single tetrahedron, the ground state manifold is connected. The parameterization of ground states in figure 4.5 demonstrates this, and guarantees that any ground state configuration on any tetrahedron can be distorted into any other continuously without leaving the ground state manifold. Further, if two spins on a tetrahedron are unconstrained, the other two can be rotated arbitrarily as long as the constraint $1 - \lambda \leq |a| \leq 1 + \lambda$ is maintained.

Maintaining this constraint is not an issue, since (by assumption) we began in a ground state and the ground state manifold is connected.

2. If two spins on a tetrahedron are held fixed, a single U(1) degree of freedom is retained for the other pair, associated with rotation about the axis given by the sum of the two fixed spins.

3. A useful special case of (1) is the following: with one spin on a tetrahedron held fixed, another can be adjusted arbitrarily and continuously (as long as the constraint $1 - \lambda \leq |a| \leq 1 + \lambda$ is maintained) if the other two spins are free.

Using these statements, we can deform any ground state into our reference state by manipulating layers of the lattice sequentially. The algorithm for doing this runs as follows.

For spins in the bottom layer of the lattice, we can, by (1), continuously adjust those tetrahedra so that $\mathbf{S}_3$ and $\mathbf{S}_4$ are in their reference configurations (4.18). This requires adjusting the configurations of spins on higher layers in order to keep every tetrahedron in a ground state configuration, but this poses no difficulties since they are unconstrained at this point.

Now that the first layer is fixed, we move on to the second. By (2), every spin in this layer is constrained to lie on a cone, and only needs to be rotated into the correct position. We can do this one by one for each tetrahedron in the bottom layer, so that they are each in the reference configuration. Note that (3) guarantees that once a tetrahedron is in its reference configuration, it will not be disturbed by adjusting spins in the same layer. As we do this, spins in higher layers can be adjusted freely to keep every tetrahedron in a ground state configuration. Importantly, we do not need to revisit spins in the first layer in this process - by (2), their fixed orientations are commensurate with the ground state constraints and the transformations required in the second layer.

This process can be repeated in every layer without difficulty. We have therefore shown that the ground state manifold of the distorted pyrochlore Heisenberg model is always connected. With this understanding established, we can now focus on the role of fluctuations in the low-

temperature limit without considering energetic obstacles.

4.4.2 Order-by-disorder in the quasi-2D limit

For a single tetrahedron, we have seen that a quasi-two dimensional limit appears for temperatures that satisfy $T \gtrsim \mathcal{O}(\lambda^2)$. This behavior persists for many-body states, essentially for the same reason that it appears in the single tetrahedron. This follows from integrating out all triangular-lattice spins, as we did in the derivation of (4.13). The resulting effective Hamiltonian is just a sum over the set of bowtie structures of terms of the form (4.13).

By the arguments provided in previous sections, the many-body configuration which is selected for $T \gtrsim \mathcal{O}(\lambda^2)$ has $\mathbf{S}_\Delta = 0$ on all kagomé triangles. In other words, the ground states of the effective many-body theory are just the ground states of the kagomé Heisenberg model on decoupled sheets. In terms of energetics, the high temperature behavior of the distorted pyrochlore Heisenberg model is essentially two-dimensional, but it is not at all obvious that this is still the case after considering the effect of fluctuations.

To study fluctuations, we once again need to develop a systematic understanding of soft modes about ground states of the effective model. A soft mode of this effective Hamiltonian corresponds to a transformation which preserves the constraint $\mathbf{S}_\Delta^2 = 0$ everywhere. Any such transformation obviously factorizes into independent transformations on every kagomé layer. This implies that the number of zero modes in a many-body state is given by, at most, the sum of the zero modes present in every kagomé layer. Our experience with the kagomé Heisenberg model naturally leads us to consider the co-planar ground states, as these contain the greatest possible number of soft modes. However, this does not provide guidance regarding the nature of inter-plane correlations, and it is possible that the ferromagnetic interactions between kagomé planes could destroy some of the zero modes.

We will now argue that this is not the case: no zero modes are destroyed by inter-plane fluctuations. Moreover, the order-by-disorder mechanism does not select for a particular form of inter-plane order. The key to this argument is to note that the effective inter-plane interactions

are of the form

$$\ln\left[\frac{\sinh(x)}{x}\right] \approx \frac{x^2}{6} \tag{4.19}$$

where $x = \beta\lambda J|\mathbf{S}_{\Delta_1} + \mathbf{S}_{\Delta_2}|$. Fluctuation corrections to the spin magnitude $|\mathbf{S}_{\Delta}|$ of order η scale as η^2, so the leading order term in the effective Hamiltonian scales as η^4. As previously discussed, all zero modes of co-planar kagomé ground states have a quartic effective potential which governs them. Since inter-plane fluctuation corrections evidently cannot restore a harmonic term, all of the co-planar quartic modes are insensitive to the presence of inter-plane interactions. The quasi-two dimensional regime mimics the thermodynamic behavior of decoupled kagomé sheets, although we should recall that for a fixed number of unit cells, the pyrochlore lattice has $4/3$ the number of spins that the kagomé does. For this reason, we predict that the quasi-two dimensional limit has a heat capacity per spin given by

$$\frac{C}{N_s} = \frac{3}{4} \times \frac{11}{12} = \frac{33}{48} \tag{4.20}$$

4.4.3 Absence of order-by-disorder at low temperatures

As mentioned previously, the pyrochlore Heisenberg model is unlike the kagomé Heisenberg model in that it does not exhibit order-by-disorder at low temperatures. The natural candidate states for selection by fluctuations on the un-distorted pyrochlore lattice are collinear states. These states support one quartic mode per tetrahedron, similar in nature to the distortion responsible for the quartic mode on every kagomé triangle discussed in Section 4.2. However, it has been demonstrated through numerical calculations that these additional soft modes are insufficient to cause selection of collinear states: in the language of (4.3), the singularity they produce in the partition function is integrable. Is order-by-disorder possible for $\lambda < 1$?

Fully collinear states are forbidden in the presence of distortion; the closest one can get to a collinear configuration is a state of the form (4.18). The defining property of these states is the fact that the triangular lattice spin is parallel or antiparallel with a kagomé spin. Tetrahedra in

these configurations support a single quartic mode, analogous to the quartic mode of undistorted tetrahedra.

These are the only geometrically privileged configurations for a single tetrahedron - coplanar order is energetically forbidden for nonzero λ. In general, other tetrahedral configurations are expected to support three quadratic modes, as a consequence of dimension counting. Four Heisenberg spins have eight degrees of freedom, and the ground state condition imposes three constraints. The ground state manifold for a single tetrahedron then has dimension five, which is parameterized by the set of global rotations and the parameters a, ϕ of figure 4.5. Anharmonic fluctuations about a ground state configuration therefore require fine-tuning. This once again leaves collinear states as the only natural candidate for order-by-disorder. However, in the distorted case, the phase space of collinear states is reduced: there can be at most one pair of (anti)parallel spins per tetrahedron, instead of two. For this reason, collinear states must produce an even more well-behaved singularity in the distorted case, and order-by-disorder does not occur.

4.4.4 Qualitative Phase Diagram

The qualitative phase diagram for the distorted pyrochlore Heisenberg model is shown in Figure 4.7. It contains the quasi-two dimensional phase without order by disorder, the disordered quasi-two dimensional phase, and the disordered three-dimensional phase. Each phase boundary is a thermal crossover.

The low temperature phases are distinguished by thermal response functions, such as the specific heat: the order-by-disorder phase has a heat capacity per spin of 33/48, while the value in the disordered three-dimensional phase is 3/4. Verifications of these predictions through numerical simulations by Monte Carlo methods would provide definitive proof that the order-by-disorder mechanism is working as described in this chapter. Another interesting subject for future work will be analysis of correlation functions in the disordered three-dimensional phase for $\lambda < 1$. We suspect that this phase is still a classical spin liquid, but this requires an investigation of co-planar

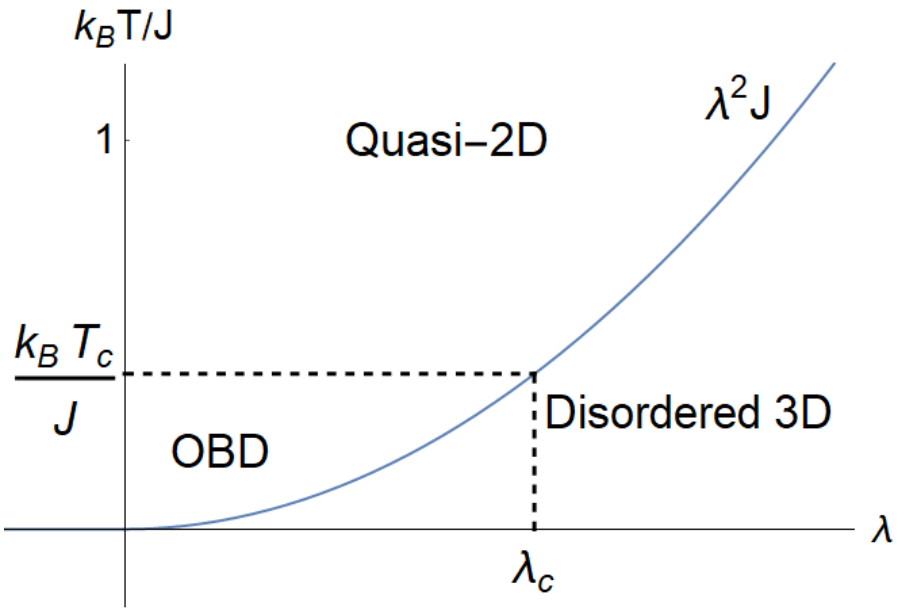

Figure 4.7: Qualitative phase diagram of the distorted pyrochlore Heisenberg model. The text "OBD" indicates the order-by-disorder regime. The scale T_c indicates the onset of the order by disorder regime in the kagomé limit, which occurs at approximately $k_B T_c \approx 0.1J$. The scale $\lambda^2 J$ can be used to estimate the critical distortion, λ_c, below which order by disorder is observable. For sufficiently small temperatures at any nonzero value of λ, the system enters a disordered three-dimensional configuration. Not shown is the crossover regime between two dimensional and three dimensional behavior, which presumably takes place over a range of temperatures.

and collinear order parameters from numerical simulations.

The class of geometric distortions discussed in this chapter is expected to be relevant to pyrochlore, or layered kagomé, systems in general. There is tremendous empirical interest in such materials in the search for quantum spin liquids, including, for example, Herbertsmithite [114]. We anticipate that this work is more directly relevant to studies of materials which exhibit classical spin-liquid behavior [115]. Although these distortions are presumably non-generic in undistorted materials, applications of different forms of strain should be able to create these conditions empirically.

Chapter 5

Concluding Remarks

Over the last few decades, condensed matter theory has been revolutionized by a sequence of remarkable discoveries. These discoveries are often empirically motivated, but it is already illuminating to consider the repercussions of those discoveries on the technical repertoire of theorists. This includes our focus on the role of topology, particularly in the context of the integer quantum Hall effect; a greater appreciation for the systematics of fractionalization in strongly correlated systems, such as frustrated antiferromagnets; and the use of gauge theories and dualities for describing interacting systems. Perhaps the most consequential among these discoveries is the existence of high-temperature superconductors, which has prompted a flood of research into their origin. Today, more than thirty years following their discovery, it is clear that many-body theory still has surprises in store for physicists.

It is unsurprising that such exotic structures are promoted by the imposition of incompatible energetic constraints. While the theory of high-temperature superconductors remains an active (and highly contentious) area of research, a broad theoretical consensus has appeared around the idea that such systems can be understood as doped Mott insulators [116]. It is therefore natural to develop theories of the parent insulating state, which has prompted a renewed interest in the theory of frustrated magnets. This dissertation has continued in this vein by considering frustrated interactions in a variety of circumstances, demonstrating the diversity of both quantum and classical phases of matter supported by such a platform. While high-temperature superconductors may well be the most exciting many-body phenomena found to date, there is little reason to doubt that frustrated magnets will continue to serve as a useful tool to search for other exotic

phases of matter. Ultracold atomic and trapped-ion systems also provide a natural and exciting extension of these ideas beyond the constraints of individual materials.

In chapter 2, we investigated how topological considerations can appear in frustrated magnets. In that context, we saw that a strongly correlated system can support exponentially localized boundary modes which are responsible for non-trivial transport properties. There has recently been significant interest in the thermal Hall conductivity (and magnon transport in general) due to its anomalous magnitude in the pseudogap phase of the Cuprate superconductors [117]. Our analysis reveals that such topological boundary modes are quite generic. Left unaddressed is the origin of topological order in the cuprates. It appears that any theory of those high-temperature superconductors must also account for this topological behavior.

Chapter 3 considered a problem which veterans of many-body theory would expect to understand well. Our model of spins on the honeycomb lattice contains an even number of spins per unit cell: such systems can often be studied accurately with the bond-operator formalism. Essentially, this class of systems are understood as analogues of Bose-Einstein Condensates in the spin channel, with a spin gap that vanishes at sufficiently large magnetic fields. Beyond that field-induced critical point, magnetic order forms. While these statements are also true for our model of Ytterbium Silicate, it seems that a previously unconsidered quantum critical point appears at the "mystery" magnetic field, H_m. At this point, the spin gap closes yet again (at least in linear spin-wave theory), and the magnetic order persists on both sides of the critical point. What role does the closing of the spin gap play in this transition? Since the transition breaks only a discrete symmetry, there is no obvious requirement that the spin gap needs to close. Understanding the properties of this quantum critical point more generally is clearly desirable, and may reveal more about the structure of the BEC dome for Ytterbium Silicate and other materials with strong spin-orbit coupling.

Finally, chapter 4 presented a theory of distorted pyrochlore antiferromagnets. This problem is essentially a classical analogue of the theory of Mott insulators or quantum spin liquids. Geometric perturbations of the type we considered can lead to an effective dimensional reduction,

which leads to qualitatively novel behavior of fluctuation-induced selection mechanisms. Experiments involving classical spin liquid compounds, such as various titanates, may well reveal the crossover behavior we described. Moreover, the consequences of such perturbations for corresponding quantum mechanical systems is of great interest. Pyrochlore systems are some of the leading candidates for observing a quantum spin liquid experimentally; if anisotropic perturbations are capable of inducing novel selection mechanisms, these need to be understood systematically in order to carry on the search for quantum liquid states. We hope that our analysis of these properties in the classical limit will help shed light on the corresponding small-spin problem.

The model Hamiltonians introduced throughout this dissertation have certainly been "simple". However, we hope that the reader can appreciate their empirical relevance - while the theory of materials can be a highly specialized business, the techniques used in our analysis are quite general. The process of constructing empirically relevant, theoretically amenable models is extremely important in the development of condensed matter physics. The examples worked out here are hopefully edifying to the reader, as there is still much to do in many-body physics. To quote X.G. Wen, "Nature never stops to surprise us" [8].

Bibliography

1 G. Hester, H. S. Nair, T. Reeder, D. R. Yahne, T. N. DeLazzer, L. Berges, D. Ziat, J. R. Neilson, A. A. Aczel, G. Sala, J. A. Quilliam, and K. A. Ross, "Novel strongly spin-orbit coupled quantum dimer magnet: $\mathrm{yb_2si_2o_7}$," *Phys. Rev. Lett.*, vol. 123, p. 027201, Jul 2019.

2 E. Fradkin, *Field Theories of Condensed Matter Physics*. Cambridge University Press, 2 ed., 2013.

3 R. Shankar, "Effective Field Theory in Condensed Matter Physics," *arXiv e-prints*, pp. cond–mat/9703210, Mar. 1997.

4 K. G. Wilson, "The renormalization group: Critical phenomena and the kondo problem," *Rev. Mod. Phys.*, vol. 47, pp. 773–840, Oct 1975.

5 J. Polchinski, "Effective Field Theory and the Fermi Surface," *arXiv e-prints*, pp. hep–th/9210046, Oct. 1992.

6 M. Kardar, *Statistical Physics of Fields*. Cambridge University Press, 2007.

7 X.-G. Wen, *Quantum Field Theory of Many-body Systems: From the Origin of Sound to an Origin of Light and Electrons*. Oxford University Press, 2004.

8 X.-G. Wen, "Quantum orders and symmetric spin liquids," *Phys. Rev. B*, vol. 65, p. 165113, Apr. 2002.

9 X.-G. Wen, "Topological order: from long-range entangled quantum matter to an unification of light and electrons," *arXiv e-prints*, p. arXiv:1210.1281, Oct. 2012.

10 J. E. Moore and L. Balents, "Topological invariants of time-reversal-invariant band structures," *Phys. Rev. B*, vol. 75, p. 121306, Mar 2007.

11 L. Savary and L. Balents, "Quantum spin liquids: a review," *Reports on Progress in Physics*, vol. 80, p. 016502, Nov 2016.

12 D. J. Thouless, M. Kohmoto, M. P. Nightingale, and M. den Nijs, "Quantized hall conductance in a two-dimensional periodic potential," *Phys. Rev. Lett.*, vol. 49, pp. 405–408, Aug 1982.

13 S.-S. Chern, "A simple intrinsic proof of the gauss-bonnet formula for closed riemannian manifolds," *Annals of Mathematics*, vol. 45, no. 4, pp. 747–752, 1944.

14 M. Nakahara, *Geometry, topology and physics*. 2003.

15 S. Sachdev, *Quantum phase transitions*. Cambridge: Cambridge University Press, second ed. ed., 2011.

16 T. Holstein and H. Primakoff, "Field dependence of the intrinsic domain magnetization of a ferromagnet," *Phys. Rev.*, vol. 58, pp. 1098–1113, Dec 1940.

17 A. Auerbach and D. P. Arovas, "Schwinger Bosons Approaches to Quantum Antiferromagnetism," *arXiv e-prints*, p. arXiv:0809.4836, Sept. 2008.

18 Y.-M. Lu, G. Y. Cho, and A. Vishwanath, "Unification of bosonic and fermionic theories of spin liquids on the kagome lattice," *arXiv e-prints*, p. arXiv:1403.0575, Mar. 2014.

19 Y.-M. Lu, Y. Ran, and P. A. Lee, "F_2 spin liquids in the $s = \frac{1}{2}$ heisenberg model on the kagome lattice: A projective symmetry-group study of schwinger fermion mean-field states," *Phys. Rev. B*, vol. 83, p. 224413, Jun 2011.

20 J. G. Rau, P. A. McClarty, and R. Moessner, "Pseudo-Goldstone Gaps and Order-by-Quantum Disorder in Frustrated Magnets," *Phys. Rev. Lett.*, vol. 121, p. 237201, Dec. 2018.

21 P. A. McClarty, X.-Y. Dong, M. Gohlke, J. G. Rau, F. Pollmann, R. Moessner, and K. Penc, "Topological magnons in kitaev magnets at high fields," *Phys. Rev. B*, vol. 98, p. 060404, Aug 2018.

22 A. Zee, *Group Theory in a Nutshell for Physicists*. USA: Princeton University Press, 2016.

23 X.-L. Qi and D. Ranard, "Determining a local Hamiltonian from a single eigenstate," *arXiv e-prints*, p. arXiv:1712.01850, Dec. 2017.

24 J. R. Garrison and T. Grover, "Does a Single Eigenstate Encode the Full Hamiltonian?," *Physical Review X*, vol. 8, p. 021026, Apr. 2018.

25 E. Chertkov and B. K. Clark, "Computational inverse method for constructing spaces of quantum models from wave functions," *Phys. Rev. X*, vol. 8, p. 031029, Jul 2018.

26 R. Orús, "A practical introduction to tensor networks: Matrix product states and projected entangled pair states," *Annals of Physics*, vol. 349, pp. 117–158, Oct. 2014.

27 M. B. Hastings, "Solving gapped Hamiltonians locally," *Phys. Rev. B*, vol. 73, p. 085115, Feb. 2006.

28 G. Kin-Lic Chan, A. Keselman, N. Nakatani, Z. Li, and S. R. White, "Matrix Product Operators, Matrix Product States, and ab initio Density Matrix Renormalization Group algorithms," *arXiv e-prints*, p. arXiv:1605.02611, May 2016.

29 L. Balents, "Spin liquids in frustrated magnets," *Nature*, vol. 464, pp. 199–208, 2010.

30 L. Pauling, "The structure and entropy of ice and of other crystals with some randomness of atomic arrangement," *Journal of the American Chemical Society*, vol. 57, no. 12, pp. 2680–2684, 1935.

31 M. Hermele, M. P. Fisher, and L. Balents, "Pyrochlore photons: The U(1) spin liquid in a S=1/2 three-dimensional frustrated magnet," *Phys. Rev. B*, vol. 69, p. 064404, Feb. 2004.

32 M. J. Lawler, "Emergent gauge dynamics of highly frustrated magnets," *New Journal of Physics*, vol. 15, p. 043043, Apr. 2013.

33 S. Sachdev, *Quantum Phases and Phase Transitions of Mott Insulators*, vol. 645, p. 381. 2004.

34 A. Y. Kitaev, "Fault-tolerant quantum computation by anyons," *Annals of Physics*, vol. 303, pp. 2–30, Jan. 2003.

35 L. Balents, "Spin liquids in frustrated magnets," *Nature*, vol. 464, pp. 199–208, 2010.

36 S. Yan, D. A. Huse, and S. R. White, "Spin-liquid ground state of the s = 1/2 kagome heisenberg antiferromagnet," *Science*, vol. 332, no. 6034, pp. 1173–1176, 2011.

37 P. Gegenwart and S. Trebst, "Spin-orbit physics: Kitaev matter," *Nature Physics*, vol. 11, pp. 444–445, June 2015.

38 P. Chandra, P. Coleman, and A. I. Larkin, "Ising transition in frustrated heisenberg models," *Phys. Rev. Lett.*, vol. 64, pp. 88–91, Jan. 1990.

39 I. Dzyaloshinsky, "A thermodynamic theory of "weak" ferromagnetism of antiferromagnetics," *Journal of Physics and Chemistry of Solids*, vol. 4, pp. 241–255, 1958.

40 T. Moriya, "Anisotropic superexchange interaction and weak ferromagnetism," *Phys. Rev.*, vol. 120, pp. 91–98, Oct. 1960.

41 A. Kitaev, "Anyons in an exactly solved model and beyond," *Annals of Physics*, vol. 321, pp. 2–111, Jan. 2006.

42 G. Jackeli and G. Khaliullin, "Mott insulators in the strong spin-orbit coupling limit: From heisenberg to a quantum compass and kitaev models," *Phys. Rev. Lett.*, vol. 102, p. 017205, Jan. 2009.

43 D. Pesin and L. Balents, "Mott physics and band topology in materials with strong spin-orbit interaction," *Nature Physics*, vol. 6, pp. 376–381, May 2010.

44 P. A. Lee and N. Nagaosa, "Proposal to use neutron scattering to access scalar spin chirality fluctuations in kagome lattices," *Physical Review B*, vol. 87, p. 064423, Feb. 2013.

45 G. Chen, T. Ma, A. T. N'Diaye, H. Kwon, C. Won, Y. Wu, and A. K. Schmid, "Tailoring the chirality of magnetic domain walls by interface engineering.," *Nature communications*, vol. 4, p. 2671, 2013.

46 G. Chen and A. K. Schmid, "Imaging and tailoring the chirality of domain walls in magnetic films," *Advanced Materials*, vol. 27, no. 38, pp. 5738–5743, 2015.

47 L. Savary and L. Balents, "Quantum spin liquids: a review," *Reports on Progress in Physics*, vol. 80, p. 016502, Jan. 2017.

48 F.-Y. Li, Y.-D. Li, Y. B. Kim, L. Balents, Y. Yu, and G. Chen, "Weyl magnons in breathing pyrochlore antiferromagnets," *Nature Communications*, vol. 7, p. 12691, Sept. 2016.

49 S. A. Owerre, "Topological transitions of magnons in three-dimensional strained chiral antiferromagnets and thermal Hall effect in honeycomb ferromagnet CrI$_3$," *arXiv e-prints*, p. arXiv:1811.01946, Nov. 2018.

50 S. A. Owerre, "Strain-induced topological magnon phase transitions: applications to kagome-lattice ferromagnets," *Journal of Physics Condensed Matter*, vol. 30, p. 245803, June 2018.

51 M. Elhajal, B. Canals, and C. Lacroix, "Symmetry breaking due to dzyaloshinsky-moriya interactions in the kagomé lattice," *Phys. Rev. B*, vol. 66, p. 014422, July 2002.

52 O. Cépas, C. M. Fong, P. W. Leung, and C. Lhuillier, "Quantum phase transition induced by dzyaloshinskii-moriya interactions in the kagome antiferromagnet," *Phys. Rev. B*, vol. 78, p. 140405, Oct. 2008.

53 T. F. Seman, C.-C. Chen, R. R. P. Singh, and M. van Veenendaal, "The many faces of quantum kagome materials: Interplay of further-neighbour exchange and Dzyaloshinskii-Moriya interaction," *arXiv e-prints*, p. arXiv:1508.01523, Aug. 2015.

54 M. Rigol and R. R. P. Singh, "Magnetic susceptibility of the kagome antiferromagnet $\mathrm{zncu_3(OH)_6cl_2}$," *Phys. Rev. Lett.*, vol. 98, p. 207204, May 2007.

55 M. Hering and J. Reuther, "Functional renormalization group analysis of dzyaloshinsky-moriya and heisenberg spin interactions on the kagome lattice," *Phys. Rev. B*, vol. 95, p. 054418, Feb. 2017.

56 V. A. Zyuzin and G. A. Fiete, "Spatially anisotropic kagome antiferromagnet with dzyaloshinskii-moriya interaction," *Phys. Rev. B*, vol. 85, p. 104417, Mar. 2012.

57 A. L. Chernyshev and P. A. Maksimov, "Damped topological magnons in the kagome-lattice ferromagnets," *Phys. Rev. Lett.*, vol. 117, p. 187203, Oct. 2016.

58 C.-Y. Lee, B. Normand, and Y.-J. Kao, "Gapless spin liquid in the kagome heisenberg antiferromagnet with dzyaloshinskii-moriya interactions," *Phys. Rev. B*, vol. 98, p. 224414, Dec. 2018.

59 S. A. Owerre, "Magnon hall effect without dzyaloshinskii–moriya interaction," *Journal of Physics: Condensed Matter*, vol. 29, p. 03LT01, Nov. 2016.

60 H. Katsura, N. Nagaosa, and P. A. Lee, "Theory of the thermal hall effect in quantum magnets," *Phys. Rev. Lett.*, vol. 104, p. 066403, Feb. 2010.

61 A. Rückriegel, A. Brataas, and R. A. Duine, "Bulk and edge spin transport in topological magnon insulators," *Physical Review B*, vol. 97, p. 081106, Feb. 2018.

62 W. Cai, J. Han, F. Mei, Y. Xu, Y. Ma, X. Li, H. Wang, Y. P. Song, Z.-Y. Xue, Z.-q. Yin, S. Jia, and L. Sun, "Observation of topological magnon insulator states in a superconducting circuit," *Phys. Rev. Lett.*, vol. 123, p. 080501, Aug 2019.

63 F. Mei, G. Chen, N. Goldman, L. Xiao, and S. Jia, "Topological magnon insulator and quantized pumps from strongly-interacting bosons in optical superlattices," *New Journal of Physics*, vol. 21, p. 095002, sep 2019.

64 M. E. Zhitomirsky and A. L. Chernyshev, "Instability of antiferromagnetic magnons in strong fields," *Phys. Rev. Lett.*, vol. 82, pp. 4536–4539, May 1999.

65 A. Mook, J. Henk, and I. Mertig, "Magnon hall effect and topology in kagome lattices: A theoretical investigation," *Phys. Rev. B*, vol. 89, p. 134409, Apr. 2014.

66 P. Laurell and G. A. Fiete, "Magnon thermal Hall effect in kagome antiferromagnets with Dzyaloshinskii-Moriya interactions," *Physical Review B*, vol. 98, p. 094419, Sept. 2018.

67 T. Yildirim and A. B. Harris, "Magnetic structure and spin waves in the kagomé jarosite compound $\mathrm{Kfe_3(SO_4)_2(OH)_6}$," *Phys. Rev. B*, vol. 73, p. 214446, June 2006.

68 K. Matan, D. Grohol, D. G. Nocera, T. Yildirim, A. B. Harris, S. H. Lee, S. E. Nagler, and Y. S. Lee, "Spin waves in the frustrated kagomé lattice antiferromagnet $\mathrm{kfe_3(OH)_6(so_4)_2}$," *Phys. Rev. Lett.*, vol. 96, p. 247201, June 2006.

69 A. L. Chernyshev, "Strong quantum effects in an almost classical antiferromagnet on a kagome lattice," *Phys. Rev. B*, vol. 92, p. 094409, Sept. 2015.

70 S. Trebst, H. Monien, C. J. Hamer, Z. Weihong, and R. R. P. Singh, "Strong-coupling expansions for multiparticle excitations: Continuum and bound states," *Phys. Rev. Lett.*, vol. 85, pp. 4373–4376, Nov. 2000.

71 M. P. Gelfand and R. R. P. Singh, "High-order convergent expansions for quantum many particle systems," *Advances in Physics*, vol. 49, pp. 93–140, Jan. 2000.

72 M. P. Gelfand, R. R. P. Singh, and D. A. Huse, "Perturbation expansions for quantum many-body systems," *Journal of Statistical Physics*, vol. 59, pp. 1093–1142, June 1990.

73 J. Oitmaa, C. Hamer, and W. Zheng, *Series Expansion Methods for Strongly Interacting Lattice Models.* Cambridge University Press, 2006.

74 S. D. Huber and E. Altman, "Bose condensation in flat bands," *Phys. Rev. B*, vol. 82, p. 184502, Nov. 2010.

75 M. E. Zhitomirsky and H. Tsunetsugu, "Exact low-temperature behavior of a kagomé antiferromagnet at high fields," *Physical Review B*, vol. 70, p. 100403, Sept. 2004.

76 S. A. Owerre, "Magnonic analogs of topological dirac semimetals," *Journal of Physics Communications*, vol. 1, p. 025007, Sept. 2017.

77 T. Fukui, Y. Hatsugai, and H. Suzuki, "Chern numbers in discretized brillouin zone: Efficient method of computing (spin) hall conductances," *Journal of the Physical Society of Japan*, vol. 74, no. 6, pp. 1674–1677, 2005.

78 R. Matsumoto, R. Shindou, and S. Murakami, "Thermal hall effect of magnons in magnets with dipolar interaction," *Phys. Rev. B*, vol. 89, p. 054420, Feb. 2014.

79 M. J. P. Gingras and P. A. McClarty, "Quantum spin ice: a search for gapless quantum spin liquids in pyrochlore magnets," *Reports on Progress in Physics*, vol. 77, p. 056501, May 2014.

80 F.-Y. Li, Y.-D. Li, Y. B. Kim, L. Balents, Y. Yu, and G. Chen, "Weyl magnons in breathing pyrochlore antiferromagnets," *Nature Communications*, vol. 7, Sep 2016.

81 J. B. Kogut, "An introduction to lattice gauge theory and spin systems," *Rev. Mod. Phys.*, vol. 51, pp. 659–713, Oct 1979.

82 A. Ortiz-Ambriz, C. Nisoli, C. Reichhardt, C. J. O. Reichhardt, and P. Tierno, "Colloquium: Ice rule and emergent frustration in particle ice and beyond," *Rev. Mod. Phys.*, vol. 91, p. 041003, Dec 2019.

83 V. Zapf, M. Jaime, and C. D. Batista, "Bose-einstein condensation in quantum magnets," *Rev. Mod. Phys.*, vol. 86, pp. 563–614, May 2014.

84 V. S. Zapf, D. Zocco, B. R. Hansen, M. Jaime, N. Harrison, C. D. Batista, M. Kenzelmann, C. Niedermayer, A. Lacerda, and A. Paduan-Filho, "Bose-einstein condensation of $s = 1$ nickel spin degrees of freedom in $\mathrm{nicl_2{-}4SC(nh_2)_2}$," *Phys. Rev. Lett.*, vol. 96, p. 077204, Feb 2006.

85 M. Kofu, H. Ueda, H. Nojiri, Y. Oshima, T. Zenmoto, K. C. Rule, S. Gerischer, B. Lake, C. D. Batista, Y. Ueda, and et al., "Magnetic-field induced phase transitions in a weakly coupleds=1/2quantum spin dimer systemba3cr2o8," *Physical Review Letters*, vol. 102, Apr 2009.

86 Y. Tsui, A. Brühl, K. Removic-Langer, V. Pashchenko, B. Wolf, G. Donath, A. Pikul, T. Kretz, H.-W. Lerner, M. Wagner, A. Salguero, T. Saha-Dasgupta, B. Rahaman, R. Valenti, and M. Lang, "Field-induced phase transition in a metalorganic spin-dimer system—a potential model system to study bose–einstein condensation of magnons," *Journal of Magnetism and Magnetic Materials*, vol. 310, no. 2, Part 2, pp. 1319 – 1321, 2007. Proceedings of the 17th International Conference on Magnetism.

87 U. Tutsch, B. Wolf, S. Wessel, L. Postulka, Y. Tsui, H. Jeschke, I. Opahle, T. Saha-Dasgupta, R. Valentí, A. Brühl, K. Remović-Langer, T. Kretz, H.-W. Lerner, M. Wagner, and M. Lang, "Evidence of a field-induced berezinskii-kosterlitz-thouless scenario in a two-dimensional spin-dimer system," *Nature communications*, vol. 5, p. 5169, 10 2014.

88 C. D. Batista and G. Ortiz, "Generalized jordan-wigner transformations," *Phys. Rev. Lett.*, vol. 86, pp. 1082–1085, Feb 2001.

89 H. Tanaka, F. Yamada, T. Ono, T. Sakakibara, Y. Uwatoko, A. Oosawa, K. Kakurai, and K. Goto, "Magnetic quantum phase transitions from gapped spin liquid state in tlcucl3," *Journal of Magnetism and Magnetic Materials*, vol. 310, no. 2, Part 2, pp. 1343 – 1348, 2007. Proceedings of the 17th International Conference on Magnetism.

90 D. S. Fisher and P. C. Hohenberg, "Dilute bose gas in two dimensions," *Phys. Rev. B*, vol. 37, pp. 4936–4943, Apr 1988.

91 E. Orignac, R. Citro, and T. Giamarchi, "Critical properties and bose-einstein condensation in dimer spin systems," *Phys. Rev. B*, vol. 75, p. 140403, Apr 2007.

92 O. Nohadani, S. Wessel, B. Normand, and S. Haas, "Universal scaling at field-induced magnetic phase transitions," *Physical Review B*, vol. 69, Jun 2004.

93 T. Giamarchi, C. Rüegg, and O. Tchernyshyov, "Bose–einstein condensation in magnetic insulators," *Nature Physics*, vol. 4, p. 198–204, Mar 2008.

94 M. Mourigal, W. T. Fuhrman, A. L. Chernyshev, and M. E. Zhitomirsky, "Dynamical structure factor of the triangular-lattice antiferromagnet," *Physical Review B*, vol. 88, Sep 2013.

95 M. E. Zhitomirsky and A. L. Chernyshev, "Colloquium: Spontaneous magnon decays," *Reviews of Modern Physics*, vol. 85, p. 219–242, Jan 2013.

96 S. R. White, "Density matrix formulation for quantum renormalization groups," *Phys. Rev. Lett.*, vol. 69, pp. 2863–2866, Nov 1992.

97 T. E. Baker, S. Desrosiers, M. Tremblay, and M. P. Thompson, "Méthodes de calcul avec réseaux de tenseurs en physique (basic tensor network computations in physics)," *arXiv preprint arXiv:1911.11566*, 2019.

98 I. Affleck, T. Kennedy, E. H. Lieb, and H. Tasaki, "Rigorous results on valence-bond ground states in antiferromagnets," *Phys. Rev. Lett.*, vol. 59, pp. 799–802, Aug 1987.

99 F. Verstraete and J. I. Cirac, "Matrix product states represent ground states faithfully," *Phys. Rev. B*, vol. 73, p. 094423, Mar 2006.

100 U. Schollwöck, "The density-matrix renormalization group," *Rev. Mod. Phys.*, vol. 77, pp. 259–315, Apr 2005.

101 U. Schollwöck, "The density-matrix renormalization group in the age of matrix product states," *Annals of Physics*, vol. 326, no. 1, pp. 96–192, 2011.

102 C. Hubig, I. P. McCulloch, U. Schollwöck, and F. A. Wolf, "Strictly single-site dmrg algorithm with subspace expansion," *Physical Review B*, vol. 91, no. 15, p. 155115, 2015.

103 R. Moessner and J. T. Chalker, "Properties of a Classical Spin Liquid: The Heisenberg Pyrochlore Antiferromagnet," *Phys. Rev. Lett.*, vol. 80, pp. 2929–2932, Mar. 1998.

104 S. Sachdev, "Kagome- and triangular-lattice heisenberg antiferromagnets: Ordering from quantum fluctuations and quantum-disordered ground states with unconfined bosonic spinons," *Phys. Rev. B*, vol. 45, pp. 12377–12396, Jun 1992.

105 U. Hizi, P. Sharma, and C. L. Henley, "Semiclassical Ordering in the Large-N Pyrochlore Antiferromagnet," *Phys. Rev. Lett.*, vol. 95, p. 167203, Oct. 2005.

106 A. Chubukov, "Order from disorder in a kagomé antiferromagnet," *Phys. Rev. Lett.*, vol. 69, pp. 832–835, Aug 1992.

107 J. Villain, R. Bidaux, J.-P. Carton, and R. Conte, "Order as an effect of disorder," *Journal de Physique*, vol. 41, no. 11, pp. 1263–1272, 1980.

108 L. Savary, K. A. Ross, B. D. Gaulin, J. P. C. Ruff, and L. Balents, "Order by quantum disorder in $\mathrm{er_2ti_2o_7}$," *Phys. Rev. Lett.*, vol. 109, p. 167201, Oct 2012.

109 M. E. Zhitomirsky, M. V. Gvozdikova, P. C. W. Holdsworth, and R. Moessner, "Quantum order by disorder and accidental soft mode in $\mathrm{er_2ti_2o_7}$," *Phys. Rev. Lett.*, vol. 109, p. 077204, Aug 2012.

110 D. Bergman, J. Alicea, E. Gull, S. Trebst, and L. Balents, "Order-by-disorder and spiral spin-liquid in frustrated diamond-lattice antiferromagnets," *Nature Physics*, vol. 3, pp. 487–491, July 2007.

111 J. T. Chalker, P. C. W. Holdsworth, and E. F. Shender, "Hidden order in a frustrated system: Properties of the heisenberg kagomé antiferromagnet," *Phys. Rev. Lett.*, vol. 68, pp. 855–858, Feb 1992.

112 R. Moessner and J. T. Chalker, "Low-temperature properties of classical geometrically frustrated antiferromagnets," *Phys. Rev. B*, vol. 58, pp. 12049–12062, Nov. 1998.

113 D. A. Huse and A. D. Rutenberg, "Classical antiferromagnets on the kagomé lattice," *Phys. Rev. B*, vol. 45, pp. 7536–7539, Apr 1992.

114 M. R. Norman, "Colloquium: Herbertsmithite and the search for the quantum spin liquid," *Reviews of Modern Physics*, vol. 88, p. 041002, Oct. 2016.

115 S. T. Bramwell and M. J. P. Gingras, "Spin ice state in frustrated magnetic pyrochlore materials," *Science*, vol. 294, no. 5546, pp. 1495–1501, 2001.

116 P. A. Lee, N. Nagaosa, and X.-G. Wen, "Doping a mott insulator: Physics of high-temperature superconductivity," *Rev. Mod. Phys.*, vol. 78, pp. 17–85, Jan 2006.

117 G. Grissonnanche, A. Legros, S. Badoux, E. Lefrançois, V. Zatko, M. Lizaire, F. Laliberté, A. Gourgout, J. Zhou, S. Pyon, T. Takayama, H. Takagi, S. Ono, N. Doiron-Leyraud, and L. Taillefer, "Giant thermal Hall conductivity from neutral excitations in the pseudogap phase of cuprates," *arXiv e-prints*, p. arXiv:1901.03104, Jan. 2019.